FLOW PATTERN IN A VERTICAL CHANNEL WITH HEATED SURFACE

Master Thesis for Indoor Environmental and Energy Engineering,
Department of Civil Engineering AAU
By Manezha Safar and Angeliki Kipourou

10/6-2015

Aalborg University
Engineering and Science
Sofiendalsvej 9-11
9000 Aalborg
Phone No.: 99 40 84 84
http://www.byggeri.aau.dk

Title:
Flow Pattern in a Vertical Channel with Heated Surface.

Project period:
IE, spring-summer 2015

Participant:
Manezha Safar
Angeliki Kipourou

Supervisor:
Olena Kalyanova Larsen
Li Liu

Editions: 5
Number of pages: 70
Completed: 10-06-2015

Synopsis:

A study will be carried out for the free convective flow in vertical channel. The investigation will be done both experimentally and analytically.
In Chapter 1, an introduction about the theory behind the convection and especially the free convection is included and the objective of that study is defined.
A literature review for all the studies that has be done to investigate the flow pattren in vertical heated channel. is presented in Chapter 2. At the end, a conclusion about how these review will be used later in the thesis is given.
In Chapter 3, the experimental data which are collected for a channel full-scale test facility will be used to validate the analytical solution obtained by CFD simulation. For all of that data velocity and temperature profiles will be presented and an indification of the convective flow regime will be done.The experimental and numerical velocity and temperature profiles will be presented and an dentification of the convective flow regime will be done.
In Chapter 4, an effort to investigate the recirculation flow analytically will be performed.
It is worth to mention that a measurement report was carried out and can be find as an appendix right after the thesis. The measuring report contains an introduction to experiment, where experiment set up , velocity and temperature measurement are explained. It has also a chapter where the definition of the necessary parameters for the analytical solution of airflow in vertical heated channel by using CFD were defined.

Preface

This report is a 4th. semester master thesis from Indoor and Environmental Engineering under the Department of Civil Engineering at Aalborg University.

In addition to this report a measuring report with appendix report is accomplished, which will be referred to as ”Appendix” and is found directly after the main report.

The report is produced by Manezha Safar, Angeliki Kipourou, students at 4th. semester, Master of Science in Indoor Environmental Engineering at Aalborg University, Spring 2015. The authors of that thesis are sincerely thankful to their supervisors, Olena Kalyanova Larsen and Li Liu for time spend during the thesis and helpful guidelines.

Readers guide

The report consists of two parts, a main report and a appendix measuring report. In the main report methods, premises and results is presented.
The appendix includes a measuring report which was done in cooperation with another student. Also there is attached a digital appendix, in the back of the main report. The digital appendix contains the results of all the cases that were carried out during the study.
Chapters in the main and appendix report are both individual chronological numbered. All the figures and tables are numbered in accordance with the chapters. Thus the first figure in chapter 2 has the number 2.1, and the second has 2.2 etc. Under every figures and tables there is a explanatory text to the figure or table. Under the figure or table there will appear a source if the pictures is not a own production. A list of all the source references is given in the bibliography list at the end of the main report. This report uses the Harvard method of bibliography with the name of the author and year of publication inserted into brackets after the text, e.g. [Lund and Condra 2011]. The source can be specific indicated in the form of a section or a part of the literature like [Lund and Condra 2011, Chap. 12]. If the source have more than two author it is indicated with "et al". The bibliography indicate the books with the author, title, issue and publisher while the web pages is indicated with author, title and the date for the download. If the source reference is positioned before a full stop it only refers to the sentence whereas if it is placed behind the full stop it refers back to the whole text section.

A source reference in the beginning of a section is valid for the whole following section unless other is stated.

Manezha Safar   Angeliki Kipourou

Resumé

I denne afhandling er det frie konvektive strømningsmønster i en lodret kanal med opvarmet overflade studeret både analytisk og eksperimentelt. Forsøgene blev udført ved et laboratorie facilitet ved Aalborg Universitet, hvor et forsøgs facilitet med en lodret opvarmet kanal blev konstrueret. Den lodrette kanal opvarmedes asymmetrisk fra en opvarmet overflade og den anden opvarmedes ved stråling fra den opvarmede flade.

Forskellige eksperimentelle tilfælde blev udført med et Rayleigh nummer, der spænder fra 3.3 $gange10^{12}$ til 12 $gange10^{12}$ og for en aspekt ratio (H / b), 8. Hastighed og temperatur målinger blev udført i kanalen. En af de vigtigste mål for denne undersøgelse er, at karakterisere strømningsmønstret i et hulrum og identificere hvilke betingelser overgang af strømmen fra laminar til turbulent sker. I denne fase, hvor der er en øget konvektion varme transport, sker fænomenet recirkulation. De eksperimentelle resultater blev brugt til at validere den numeriske løsning, som opnås ved hjælp af den turbulente reliazable k - $epsilon$ model. Sammenligning af de eksperimentelle og numeriske data i form af hastighed og temperaturprofiler langs kanalen præsenteres.

Abstract

In this thesis the free convective flow pattern in a vertical channel with heated surface is studied both analytically and experimentally. The experiments were performed at the labaratory facility of Aalborg University, where a test facility of a vertical heated channel was created. The vertical channel was heated asymmetrically from a heated suface and the other one is heated only by radiation from the other. Different experimental cases were performed with a Rayleigh number ranging from 3.3×10^{12} to 12×10^{12} and for an aspect ratio (H/b) of 8. Velocities and temperatures measurements were conducted in the channel. One of the main goal of that investigation is to characterise the flow regime in a cavity and to identify under which conditions the transition of the flow from laminar to turbulent happens. In that phase, where there is an increased convection heat exhange, the recirculation phenomenon happens. The experimental results were used to validate the numerically solution, which is obtained by using the reliazable k-ϵ as a turbulent model. Comparison of the experimental and numerical data in the form of velocity and temperature profiles along the channel are presented.

List of symbols

Symbol	Unit	Name
ACH	h^{-1}	Air change rate
Re	$-$	Reynolds number
Ra	$-$	Rayleigh number
Pr	$-$	Prandtl number
Gr	$-$	Grashof number
Gr_y	$-$	Grashof number in of point y
Ri	$-$	Richardson number
Ts	Kor°C	Temperature of the surface
T	Kor°C	Temperature of the fluid
l	m	Characteristic Lenght
b	m	Width of the channel
H	m	Hight of the channel
D_h	m	Hydraulic diameter
g	m^2/s	Gravitational acceleration
u	m/s	Velocity
C_p	$J/(KgK)$	Specific heat capacity
nu	m^2/s	Kinematic vicosity of the fluid
mu	$N \cdot s/m^2$	Dynamic viscosity of the fluid
ρ	Kg/m^3	Density
ρ_0	Kg/m^3	Constant density of the flow
β	k^{-1}	Thermal volumetric expansion coefficient
δ	m	Thickness of the boundary layer
ϵ		Dissipation rate
$\sigma_k - \sigma_\epsilon$		Turbulent Prandtl numbers for k and ϵ

Symbol	Unit	Name
k		Turbulent kinetic energy
S_ϵ		Source term
Y_M		Countribution of the fluctuating dilatation in compressible turbulence to the overall dissipation rate
G_b		Generation of turbulent kinetic energy due to the bouyancy
G_k		Generation of the turbulent kinetic energy due to the mean velocity gradients
Y	m	Local y-coordinate of the point
t_i	$Kor°$C	Measured temperature at point i
t_{out}	$Kor°$C	Measured temperature at the outlet
t_{SP}	$Kor°$C	Set point temperature used for the heaters
ΔT	$Kor°$C	Temperature difference
DSF		Double Skind Facade
CFD		Computational Fluid Dynamic

Table of contents

List of Tables

List of Figures

CHAPTER

1 Introduction

Heat transfer is a process of thermal energy movement. Scientific laws dictate that such energy will always seek equilibrium and move from substances of high energy to the substances with low energy trying to make their thermal energy equal.

Thermal energy is always moving. No matter what substance is heated, there is always a different place for the heat to move unless all of the available agents are the same temperature, and equilibrium is achieved. Some substances manage to hold onto their heat longer than others. Substances with similar temperatures will exchange heat more slowly, while substances with a large temperature difference, such as air and fire, will exchange heat very quickly. The process, which uses thermal heat to travel through a substance, and between a substance and another, is basically the same, but it is divided into three different categories such as heat transfer by conduction, convection and radiation. The aim of this project is to study the convective heat transfer. Convection occurs when a fluid comes in contact with a heated surface, it gets heated up and begins rising due the decrease of the density. In case of fluid heating inside a vertical channel, the fluid density decreases so it becomes lighter. This density difference between the fluid and the heated surface, drive the fluid upwards. The flow mechanism on a heated surface can be divided into three types: free or natural convection, forced convection and mixed convection. In natural convection, the fluid motion is driven by the buoyancy forces created by temperature difference. The forced convection is caused by external forces like the pressure gradient or the flow speed while the mixed convection is a combination of the natural and forced convection. The two main flow types found in both forced and free convection are laminar and turbulent. [Michael Andersen, 2014]

In laminar flow type the fluid flows in good order and it is possible to identify the streamlines along which the fluid particles move. The flow is laminar for small velocities and by increasing the velocity it gets more restless and become turbulent.
If one consider a flat vertical plate it is known that the boundary layer thickness grows and that the velocity gradients at x = 0 decrease in stream-wise (y-axis) direction. The highly ordered behaviour continues until a transition zone is reached, above which a conversion of flow from laminar to turbulent occurs, see figure fig:transi (it is important to mention that the figure describes the flow in a horizontal surface, but the mean principle are the same in vertical surfaces as well).

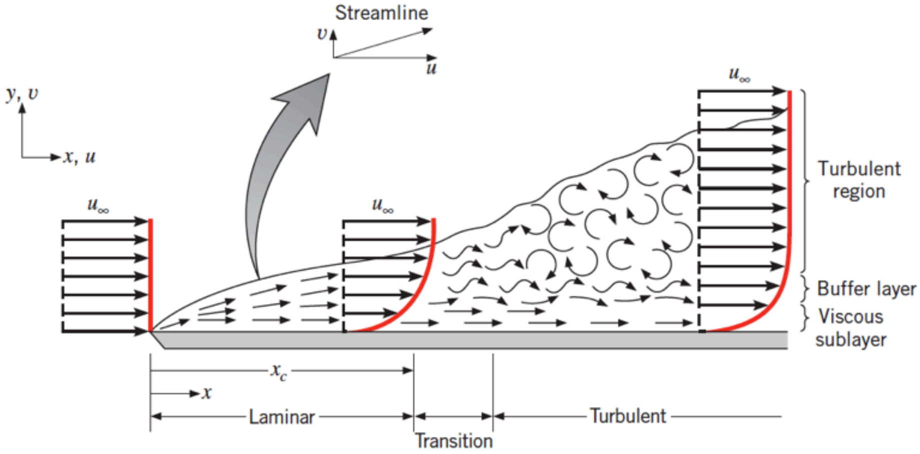

Figure 1.1. Boundary layer by laminar- and turbulent flow over a flat surface [Incropera, Frank P, 2011].

As it can be seen the fluid flow adjacent to the wall surface is laminar in a boundary layer that increases its thickness with distance. The boundary layer may become turbulent despite the fact that the flow could remain laminar in a thin layer close to the surface. *Once the flow becomes turbulent, the eddying motion carried the bulk particles of fluid across the main direction of flow, a more effective mixing mechanism and heat transfer coefficients in turbulent flow are greater than those for laminar flow* [Davies, Morris Grenfell, 2004]. No matter if the flow is laminar or turbulent, at a finite distance if the channel size allows this, the boundary layers merge and both velocity and temperature gradients vanish. In this case the flow can be described as fully developed.
Now it can be concluded that the range of the convection heat transfer depends on the development of the boundary layers and is divided into three different situations:

1. when the space between the parallel vertical plates is so large, that the development of the boundary layer on each plate is independent and develops along the height without interacting with the boundary layer of the other vertical solid surface.
2. when the space between the parallel plates is restricted and the cavity width is much lower than its height, it is expected that the boundary layers will be merged at some height and a fully developed flow will occur.
3. between the previous two situation there also another one transitional situation in which the boundary layers interacts with each other but their temperature and velocity profile are still developing before reaching the second situation with merged boundary layers.

It is worth to mention that in the transition part of the flow just before the laminar becomes turbulent a recirculation occurs. Convection heat transfer is affected by recirculation occurrence causing deformation of the vertical temperature gradient that will affect the buoyancy forces in naturally ventilated cavity. When the buoyancy forces become so large that natural convection begins to dominate the flow recirculation process takes place, and as a result creates a field in the channel with the minimal pressure that causes flow to reverse. [Gau, C and Yih, KA and Aung, Win, 1992]

The main objective of the thesis is to investigate the airflow phenomena which happen due to convection both experimentally and numerically. The used geometry for the study of the convective heat transfer is a vertical channel, formed by two parallel solid surfaces. The thermal boundary conditions are asymmetric with one wall being uniformly heated (by electrical heating mats) providing the necessary temperature differences for the buoyancy driven flow and the other was made of glass with high thermal conductivity.

The convective airflow pattern with different heat inputs and ACH will be studied. Moreover, an effort will be done to create the necessary flow regime in order for the recirculation phenomenon to take place.

The results obtained from the experiment will be used to validate the analytical solution which will be derived by the usage of Computational Fluid Dynamics (CFD). This CFD analysis, if it validates the experimental flow pattern with accuracy, could be used as a benchmark for studying the thermal performance and the recirculation phenomenon in a vertical channel.

CHAPTER

2 Literature Review

Before continue with the literature review, it is needed to mention some dimensionless numbers that are widely used for the heat transfer in vertical channels and they were presented by [Incropera, Frank P, 2011]. It needs to be mentioned that this analysis with dimensionless numbers does not solve the flow equations but it gives the characteristics of the flow.

Reynolds number (Re)

The Reynolds number represents the ratio of the inertial forces to viscous forces in a region of characteristic length l. It is given by the equation 2.1 and it can characterize the flow regime.

$$Re = \frac{u \cdot l}{\nu} \tag{2.1}$$

Where:

u	Velocity [m/s]
ν	Kinematic viscosity of the fluid [m_2/s]
l	Characteristic length [m]

Prandtl number (Pr)

The Prandtl number is the ratio of the momentum diffusivity to the thermal diffusivity, it is given by the equation 2.2 and it depends on the properties of the fluid. It gives information about the thickness of the velocity and thermal boundary layer. When Pr=1, then the thicknesses of velocity and thermal boundary layer are of the same order of magnitude [Schlichting, Herrmann and Gersten, Klaus and Gersten, Klaus, 2000].

$$Pr = \frac{C_p \cdot \mu}{k} \tag{2.2}$$

Where:

C_p	Specific heat capacity of the fluid [$J/kg \cdot K$]
μ	Dynamic viscosity of the fluid [$N \cdot s/m^2$]
k	Thermal conductivity of the fluid [$W/m \cdot K$]

Grashof number (Gr)

The Grashof number can be interpreted as the ratio of the buoyancy forces to viscous forces and it can characterize the flow regime in natural convection. It can be said that it plays a similar role in free convection as the Reynolds number plays in forced convection. It is defined as:

$$Gr = \frac{g\beta(T_s - T_\infty)l^3}{\nu^2} \tag{2.3}$$

Where:

g	Gravitational acceleration [m^2/s]
β	Thermal volumetric expansion coefficient [k^{-1}]
ρ	Fluid density [kg/m^3]
ν	Kinematic viscosity of the fluid [m^2/s]
T_s, T_∞	Temperature of the surface and the fluid [K]
l	Characteristic length [m]

[Wirtz, RA and Stutzman, RJ, 1982] at their study, they took into consideration in Grashof number the width of the cavity *b* and the aspect ratio of the cavity *b/H*. The equation of Grashof number was formulated as it can be seen in the equation 2.4.

$$Gr = \frac{g\beta(T_s - T_\infty)b^3}{\nu^2}\frac{b}{H} \tag{2.4}$$

Based on this equation, they found correlations to characterize the development of the flow convective heat transfer into the three different situations:

$1000 < Gr$	Development of the flow as it happens for a single plate
$0 < Gr < 0.2$	Fully developed flow
$0.2 < Gr < 1000$	Developing flow (Transitional)

Rayleigh number (Ra)

The Rayleigh number is the product of Grashof and Prandtl number and it is used to find the strength of free convection.

$$Ra = Gr \cdot Pr \tag{2.5}$$

Richardson number (Ri)

In order to find if the convection phenomenon is assisted or naturally driven the Richardson number is used which is a ratio of buoyancy forces to inertial forces and it characterizes the flow regime.

$Ri = \frac{Gr}{Re^2} << 1$	Forced convection
$Ri = \frac{Gr}{Re^2} \approx 1$	Mixed convection
$Ri = \frac{Gr}{Re^2} >> 1$	Free convection

Many studies have be done to investigate the heat transfer from a vertical channel due to its widely usage. The more recent studies was focused on turbulent natural convection of vertical channel.

[Yilmaz, 2007] investigated numerically and experimentally the characteristics of turbulent flow in a vertical channel with asymmetric heating. One channel wall was heated with uniform heat flux and the opposite was adiabatic. Three different Rayleigh number were used *Ra (b/h)*, 1.91×10^7, 2.74×10^7, 13.19×10^7 for a channel aspect ratio of 1/20. The numerical data had some small differences with the experimental data. For the numerical data a LRN $k-\epsilon$ turbulence model were used for the solution. The model was able to predict the mean temperature distribution but it overestimated the velocities especially in the core region of the channel cavity. They also found that in the range of *Ra(b/h)* below 105, there were indications for transitional flow from laminar to turbulent.

[Badr, HM and Habib, 2006] worked on the numerical simulation of the turbulent free convection in a channel with isothermal or isoflux heating conditions to obtain the details of the flow and its thermal characteristics. They covered a range of Rayleigh numbers from 10^5 to 10^7 for different geometrical aspect ratios (from 12.5 to 100). The analytical results for Rayleigh number has been plotted and it shows a velocity profile with one peak close to each wall. These velocity peaks become sharp and move towards the channel walls with the increase of the modified Rayleigh number. It means that the vertical velocity component increases across the channel as Rayleigh number increases causing an increase in the mass flow rate as expected. This study also indicates that as Rayleigh number increases the local Nusselt number also increases due to decrease of the thermal layer thickness. A comparison of their analytical results with the experimental results conducted by [Miyamoto, 1982] were performed and they found correlations to express the Nusselt number in terms of Rayleigh number and geometrical aspect ratio. They mentioned a difference in the velocity profiles between the analytical and experimental data and the analytical low Re turbulent model could not predict the velocity profiles in regions with high velocity gradients.

[Ayinde, 2008] did velocity measurements using the Particle Image Velocimetry (PIV) system in an anti-symmetrically heated vertical channel. One plate was heated uniformly above the ambient temperature and the other plate was kept below ambient temperature. According to these measurements a flow recirculation in the channel cavity was found as result of the flow moving along the hot wall and downward along the cold wall. They developed a correlation for the dimensionless flow rate.

[Alzwayi, Ali Saad, 2013] tried to study numerically the transition in vertical channel and how it was affected by the merging of the two boundary layers by using three different $k-\epsilon$ model for different aspect ratios, angular orientation of the walls. From the $k-\epsilon$ models, the Realizable model with an enhanced wall function was in better agreement with some published experimental data. As for the angular orientation of the wall, it was proved that when the angle increased, the transitional phase moved further downstream of the channel.

The study of the heat transfer in vertical channels also concerns the building sector since it can be used as it was mentioned in chapter 1 on page 1 in buildings for heating and cooling. In the PHD [Kalyanova, Olena], the thermal and energy performance of a Double Skin Façade which works like a vertical channel was investigated experimentally. Free and forced convection took place. For the vertical temperature profiles, it was found they had changes due to the increased heat transfer taking place at the transition between laminar and turbulent flow. An interesting explanation of the recirculation flow was described. When the ambient air is entering into the cavity and has contact with the heated surface, there is a development of the boundary layer caused by the viscous forces and it will increase with increasing distance from the inlet. Because of the high temperature difference between the heated surfaces and the fluid, the velocity of the air inside the boundary layers will be higher than the velocity of the core region of flow. Due to the mass balance, the further development of the boundary layers can occur only at the expense of the main flow. Therefore while the velocities in the boundary layers are increasing, the velocities in the main flow are decreasing. As a result of this, the boundary layers in order to continue developing they reach a stage when the mass flow entering the cavity is equal to the boundary layers flow (it happens in the Recirculation neutral plane RNP). Above this neutral plane, the flow inside the boundary layers is bigger than the entering mass flow. So, they boundary layers can continue developing only with air that *it will be drawn from the zones above RNP, causing a recirculation flow in the centreline of the cavity*.

In the article [Bacharoudis, Evangellos, 2007] the heat transfer from free convection in a solar chimney was studied experimentally and analytically. For the analytical solution six different $k-\epsilon$ turbulent models were used. The more suitable was found to be the Realizable $k-\epsilon$ model with enhanced wall treatment for the laminar sublayer in the turbulent flow. The measurements were executed for a Ra number of 1.04×10^{11}.

As a conclusion, it can be said that free convection had been widely investigated by many researchers for many geometries of interest since it has a wide range of applications in many sectors. The studies were both analytical and experimental. Most of them they were focused on turbulent or laminar flow regime, without taking into account the transitional regime which occurs between the laminar and turbulent flow. Where according with some studies the recirculation phenomenon takes place. Only few of them could be found in literature. By taking into account what had been done earlier, an effort will be done to create this transitional flow regime experimentally with high Grashof numbers. Moreover, a CFD simulation will be carried out by having as a benchmark what had been done in literature in similar cases, to predict the airflow and its flow regime.

CHAPTER

3 Results

The air flow in a vertical channel was studied experimentally and numerically. The experiments were conducted with cooperation of another student. Therefore, the description of the measurements set-up can be found in appendix . In addition, all the decisions regarding to the numerical simulation are presented as well in appendix .
In this chapter, different cases will be presented and the results obtained experimentally and numerically will be analysed.

3.1 Case Description

In order to study the flow in a vertical heated channel there has been performed 13 experiments.The measurements for all experiments were conducted in a vertical channel with a width of 0.4 m and an aspect ratio *b/H* of 1/8 and the range of the Rayleigh number in all measurements are 3.3×10^{12} to 12.0×10^{12}. An overview of all performed tests can be seen in table 3.1. It is worth to mention that the heaters in all the measured cases had temperatures almost 4 °C less than the set point.

All the tests were divided in 4 groups according to the their temperature set point and air change rate (ACH). The first group consists of four tests with constant temperature set point but ACH changed from 1 h^{-1} to 5 h^{-1}. The next group contains four tests that have the same ACH but the temperature set point was changed from 35 ° C to 53 ° C. The third group contains only two tests and has again the same temperature of 53 ° C and different ACH. The last group includes four tests. In this group a temperature gradient in the channel had been conducted and ACH was ranging from 1.5 h^{-1} to 10 h^{-1}.

It is worth mentioning that all test were performed for a cavity of 40 cm and also the heater that was placed in the bottom of the channel did not work from test number 9.

During the experiment it was observed that the heaters were unstable and their response to reach the desired temperature each time was slow. Especially for the heater at the height of 2.25 m, these fluctuations were sometimes more than 2.8 °C.

	Test Number	Temperature [C]	ACH [1/h]	Inlet Temperature [C]	CFD
Group 1	5	35	5	25.7	
	6	35	3	25.5	
	7	35	1.5	24.6	+
	8	35	1	25.7	
Group 2	7	35	1.5	24.6	+
	9	39	1.5	25.4	
	10	45	1.5	28.6	+
	11	49	1.5	29.5	
	12	53	1.5	29.3	
Group 3	12	53	1.5	29.3	+
	13	53	10	26.3	+
Group 4	1	33-36-39-42-45	1.5	25.2	
	2	33-36-39-42-45	5	25.2	
	3	33-36-39-42-45	10	25.1	
	4	33-36-39-42-45	3	25.2	

For the analysis of the results, a representative case was chosen to be analysed in the sections 3.4 on page 15, 3.5, 3.6 and 3.7. The results of all the other cases are included in the electronic appendix C on page 51.

3.2 Convection Regime

The ratio of Grashof and Reynolds number which characterises the convective flow regime was decribed in chapter 2 on page 5. The mean driving forces in this case as mentioned before was buoyancy since there was no external forces that could influence the flow.

For calculation of Grashof number the equation 2.4 on page 6 was used. And for the Reynolds the equation 2.1 on page 5 was used. The characteristic length in the equation can be defined either in terms of the cavity width b or in terms of the channel length l or in terms of the hydraulic diameter D_h. In this study the height of the channel was used as the characteristic length.

For the calculation of Grashof number the measured temperatures between the surfaces and all the points in the cavity were taken into account. These points were located where thermocouples had been placed according to appendix A.4. Grashof numbers had been calculated from both surfaces. The following graphs show an overview of Gr/Re^2 - ratio for all 4 groups.

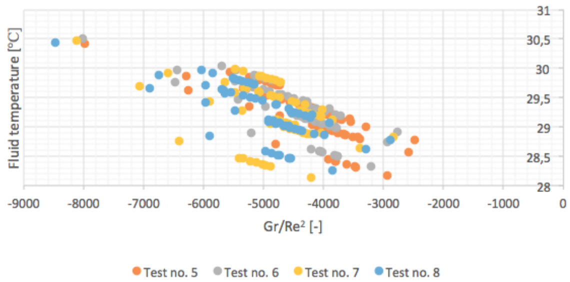

Figure 3.1. Gr/Re^2 - ratio for group 1 calculated from the glass surface.

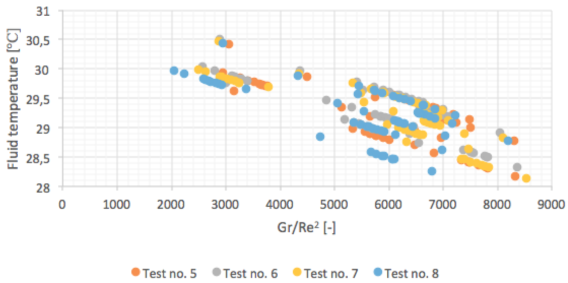

Figure 3.2. Gr/Re^2 - ratio for group 1 calculated from the heater surface.

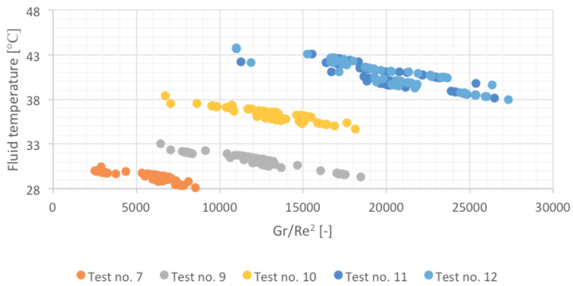

Figure 3.3. Gr/Re^2 - ratio for group 2 calculated from the glass surface.

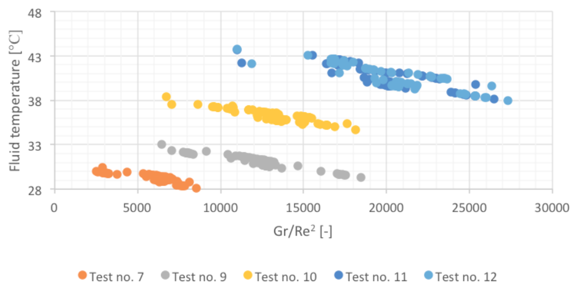

Figure 3.4. Gr/Re^2 - ratio for group 2 calculated from the heater surface.

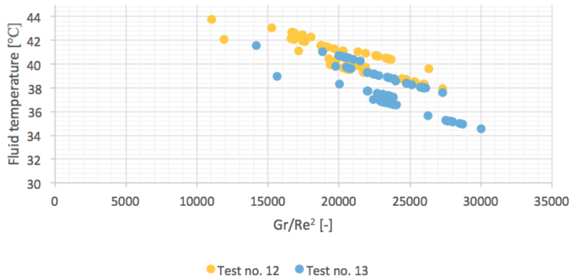

Figure 3.5. Gr/Re^2 - ratio for group 3 calculated from the glass surface.

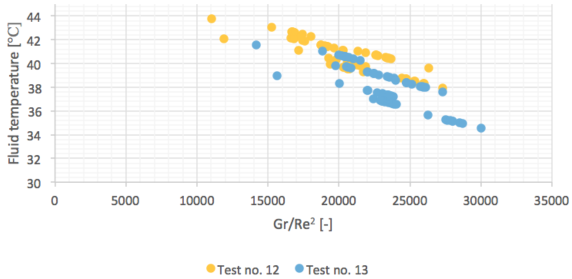

Figure 3.6. Gr/Re^2 - ratio for group 3 calculated from the heater surface.

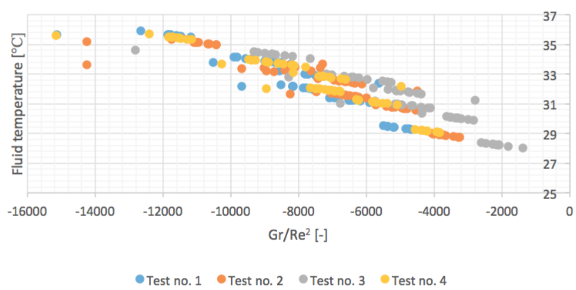

Figure 3.7. Gr/Re^2 - ratio for group 4 calculated from the glass surface.

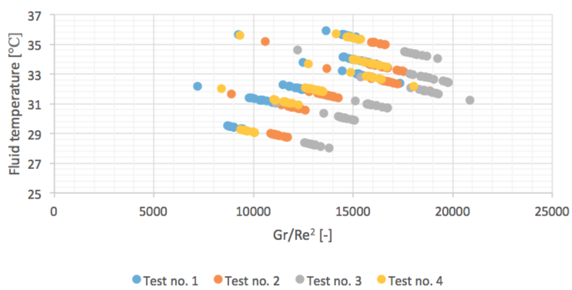

Figure 3.8. Gr/Re^2 - ratio for group 4 calculated from the heater surface.

The negative values for Gr/Re^2 - ratio were caused, because the temperature on the glass surface is lower than the fluid temperature.
As mentioned earlier in this chapter group 1 and 2 had the same set point but different ACH. In group 1 it can be observed that high ACH gave lower value of Gr/Re^2 - ratio. High ACH meant high velocity and high velocity gave high values of Reynolds number, which also means increasing of buoyancy effects in the channels.
The convection regime in all groups was buoyancy dominated and thereby can be identified as free convection regime. For better indication a comparison of the groups were done in the following figue3.9 from [Kalyanova, Olena].

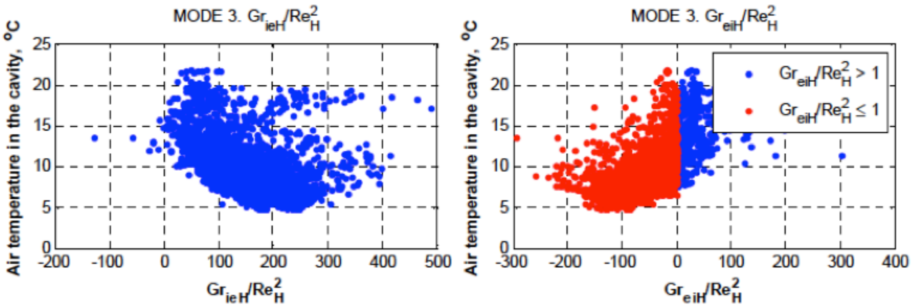

Figure 3.9. Overview of Gr/Re^2 - ratio. [Kalyanova, Olena]

As it can be observed the tendency of the graphs were almost the same as it is on the figure 3.9, but they had a low ratio of Gr/Re^2 because the velocity that was used in the thesis were high.

3.3 Flow Regime

Rayleigh number was used to determine if the flow is laminar or turbulent. Rayleigh number as mentioned before is a dimensionless number that is defined as a product of Grashof number, which describes the relation between buoyancy and viscosity within a fluid and the Prandtl number. Rayleigh number for all the groups are found by using equation 2.5 on page 6 and presented in this section.

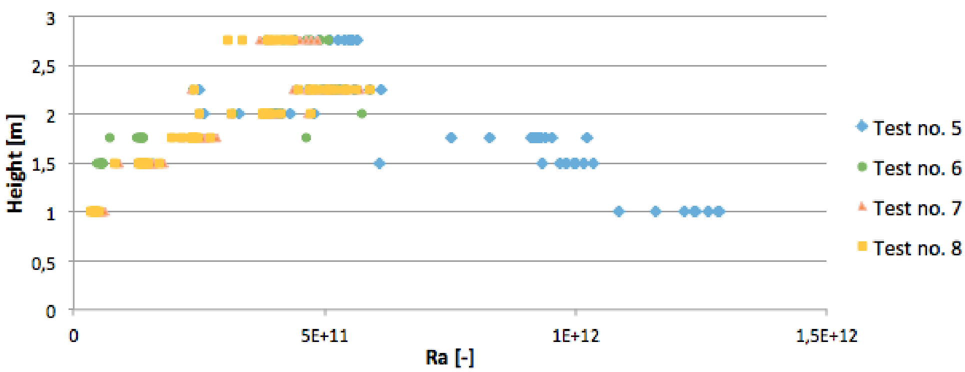

Figure 3.10. Local Rayleigh number for group 1 calculated from the hearter surface.

The figure 3.10, where the temperatures were constant but the ACH were different for each tests shows that with temperature changes the distribution of Rayleigh number changed as well. Test number 5 had the highest ACH and it can be observed that it had the greatest value of Rayleigh number. It is also worth to mention that the points closest to the heater surface in every test had the greatest value of Rayleigh number. According to [Incropera, Frank P, 2011] the transition between laminar and turbulent flow is correlated in terms of Rayleigh number and the critical point is when Ra = 10^9. In the above graphs it is observed that the Rayleigh number varied from $1x10^9$ to $1.5x10^{12}$ which means that the Rayleigh number was higher than the critical point in all the tests thus the flow was turbulent. It can be concluded that high ACH and high temperature gives higher value of Rayleigh number.

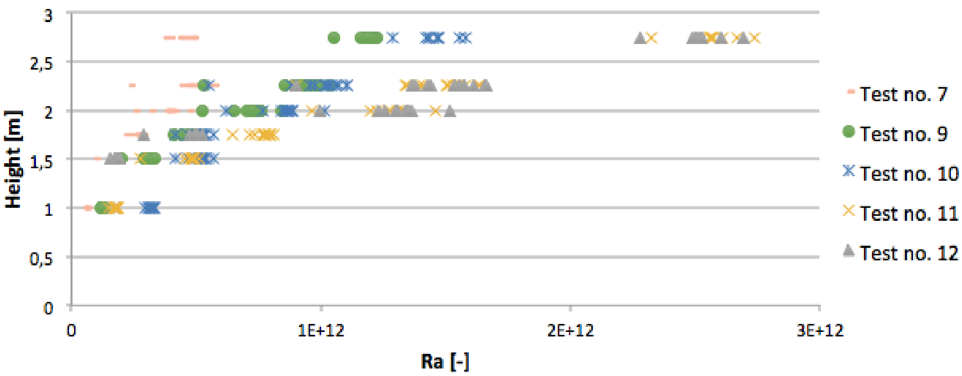

Figure 3.11. Local Rayleigh number for group 2 calculated from the heater surface with a ACH of 1.5 1/h and a temperature that changes from 35°C to 53 °C.

In test 7 and in tests 9 to 12 the air flow was constant in the channel, while the air temperature varied from 35°C to 53 °C. It can be observed that the flow in the boundary layer had more turbulent by the change of temperature from lowest to the highest, see figure 3.13.

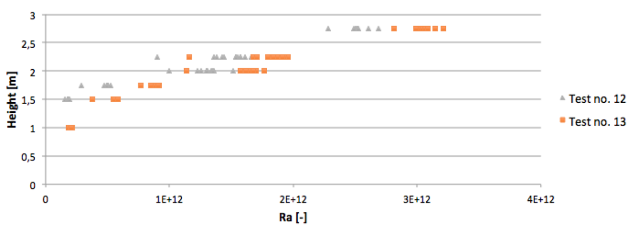

Figure 3.12. Local Rayleigh number for group 3 calculated from the heater surface with a temperature of 53 °C and ACH that of 1.5 h^{-1} and 10 h^{-1}.

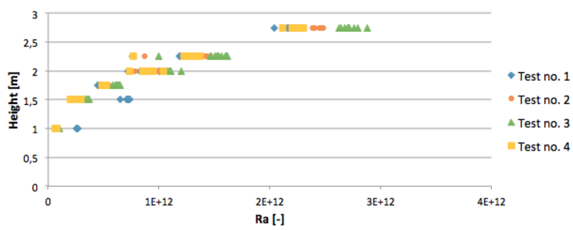

Figure 3.13. Local Rayleigh number for group 4 calculated from the heater surface with different temperature set point and different ACH.

Test 13 in figure 3.12 had the highest temperature set point and ACH thus it had the greatest Rayleigh number. Here the flow in the boundary layers was getting very turbulent compared to the rest of the tests. In tests 1 to 4 in figure 3.13 both ACH and temperature changed in each height of the channel, see chapter 3.1 on page 10. Once again it shows that flow gets more turbulent with highest temperature and ACH.

In natural convection in a channel flow the modified Grashof number according to the equation 2.4 on page 6 was calculated. The flow regime inside the cavity can be divided according to the three regions that were written in Chapter 2 on page 5. In the first situation that in general happening near the entrance region of the fluid,with the modified $Gr > 1000$, the thermal boundary layers are developing. In that situation, the velocities are higher near the walls and the biggest part of the fluid remains at the ambient temperature. The heat transfer is like the one of a single vertical wall. In the second situation when the formulated Grashof number is between $0.2 < Gr < 1000$, the boundary layers have been merged despite the fact that the velocities near the walls are still higher. This is described as a transitional regime between the flow characteristic of a single plate and the flow characteristics of a channel flow. When $0 < Gr < 0.2$, the flow can be described as fully developed flow, where boundary layers do not longer exist and the mean flow velocity profile does not change anymore in the direction of the flow. The calculated modified Grashof number for tests 1 to 8 is showed in figure 3.14 for glass surface and in figure 3.15 for heater surface.

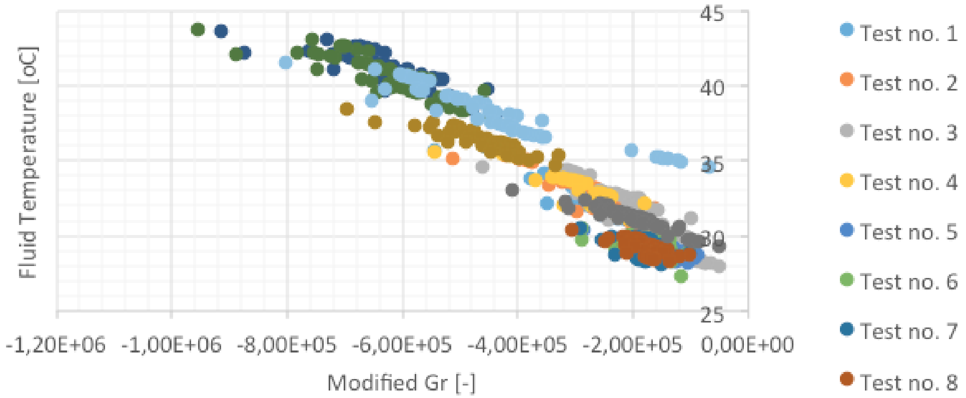

Figure 3.14. Modified Grashof number calculated from glass surface.

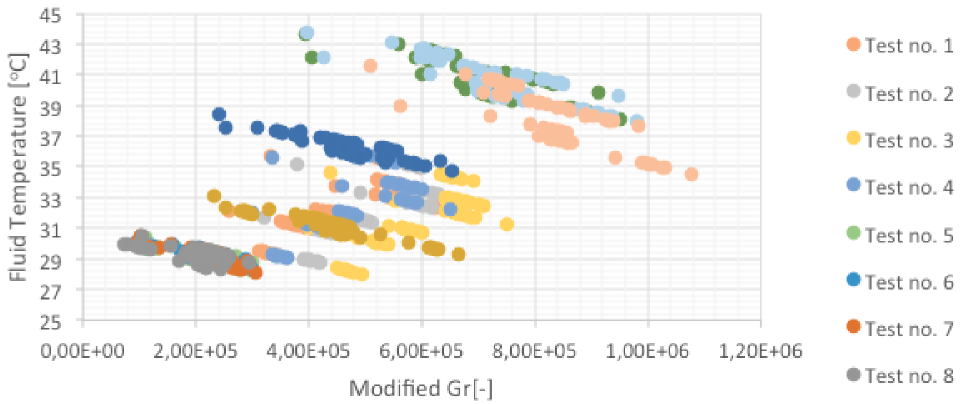

Figure 3.15. Modified Grashof number calculated from heater surface.

According to figures and all the previous mentioned, the boundary layers were being developed as single plates for both surfaces.

3.4 Thickness of the Boundary Layers

The thickness of the turbulent boundary layers were calculated by the equation proposed by [Eckert, ER and Jackson, Thomas W, 1950] and is given in the equation 3.1.

$$\delta = 0.566 \cdot y \cdot Gr^{-\frac{1}{10}} \cdot Pr^{-\frac{8}{15}} \cdot [1 + 0.494 \cdot Pr^{\frac{2}{3}}]^{\frac{1}{10}} \tag{3.1}$$

Where:

δ	Thickness of the boundary layer [m]
Y	Local y coordinate of the point [m]
Gr_y	Grashof number of point y [−]
Pr	Prandtl number [−]

The equation had been derived after the investigation of the flow and heat transfer in a turbulent free convection boundary layer on a vertical flat plate with constant temperature difference between the surfaces and ambient. The equation was found to have a good agreement with experimental data for a fluid with Prandtl number near 1 and Grashof number ranging from 10^{10} to 10^{12}. Their correlation was derived by taking into account the movement of the boundary layer as a whole instead of studying the movement of each particle of the boundary layers. According to [Heiselberg, Per and Sandberg, Mats, 1990] it was proved that this error can be acceptable and the equation can be used.
The boundary layers of the experimental cases were calculated from the equation 3.1 by using the temperature measurements. The used y coordinates were the heights of the location of the thermocouples as it is illustrated in figure A.4 on page 38 in the Appendix. These heights were 0.25, 1.00, 1.50, 1.75, 2.00, 2.25 and 2.75 m. The temperature difference used for the calculation of Grashof numbers at each height were calculated by taking the difference between the surface temperatures (both from heaters and glass) and the temperature in the middle of the cavity at each height. As for the simulated cases, the temperatures were taken from the solution data of each simulation for the same points, the thickness were calculated at the same way as it was previously described for the experimental cases. In figure 3.16 the thickness of the boundary layers from both numerical and experimental results of the case number 12 with a set point of 53 °C and an ACH of 1.5 h^{-1} is illustrated.

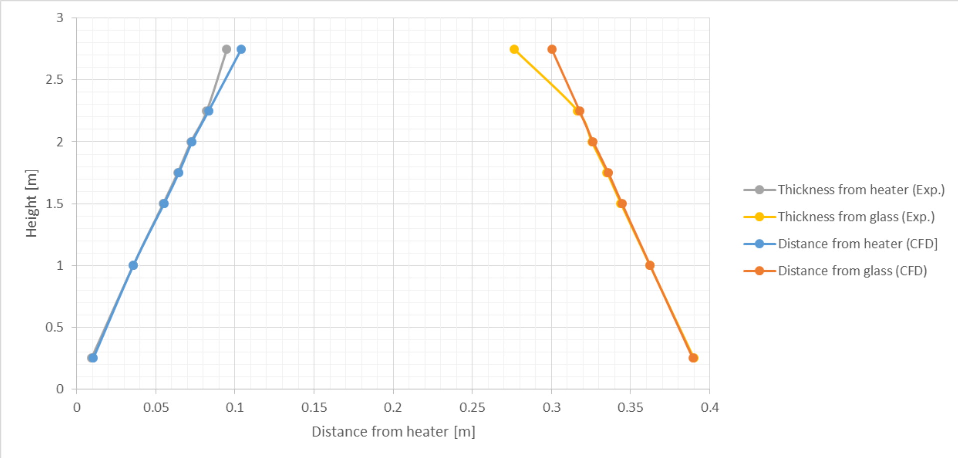

Figure 3.16. The thickness of the boundary layers obtained from numerical and experimental results.

It can be said that both the boundary layers were developing along the cavity and without influencing each other. Their thickness was increasing with increasing distance from the entrance. They were being developed as a single flat plate for both the experimental and numerical results and the flow in the cavity had not been fully developed. According to the experiment, the thickness of the boundary layers of heated and glass surface were developing almost evenly distributed along the height and both of them had a thickness of 0.12 m at the highest measured point. The thickness of both boundary layers were the same according to the results obtained from the simulations. This was expected because as it will be explained later in section 3.5 the simulated and experimental temperatures were in a good agreement.
As for the thickness of both boundary layers at the highest measured point, it had a slight difference between the experimentally and analytically calculated thicknesses. It may be happen due to the fact that the outlet boundary conditions were not defined very accurate at CFD simulation.

3.5 Horizontal Temperature Profiles

The horizontal temperature profiles were created from the experimental and numerical data to investigate further how the air flow developed in the cavity along the height and they are illustrated in figure 3.17.

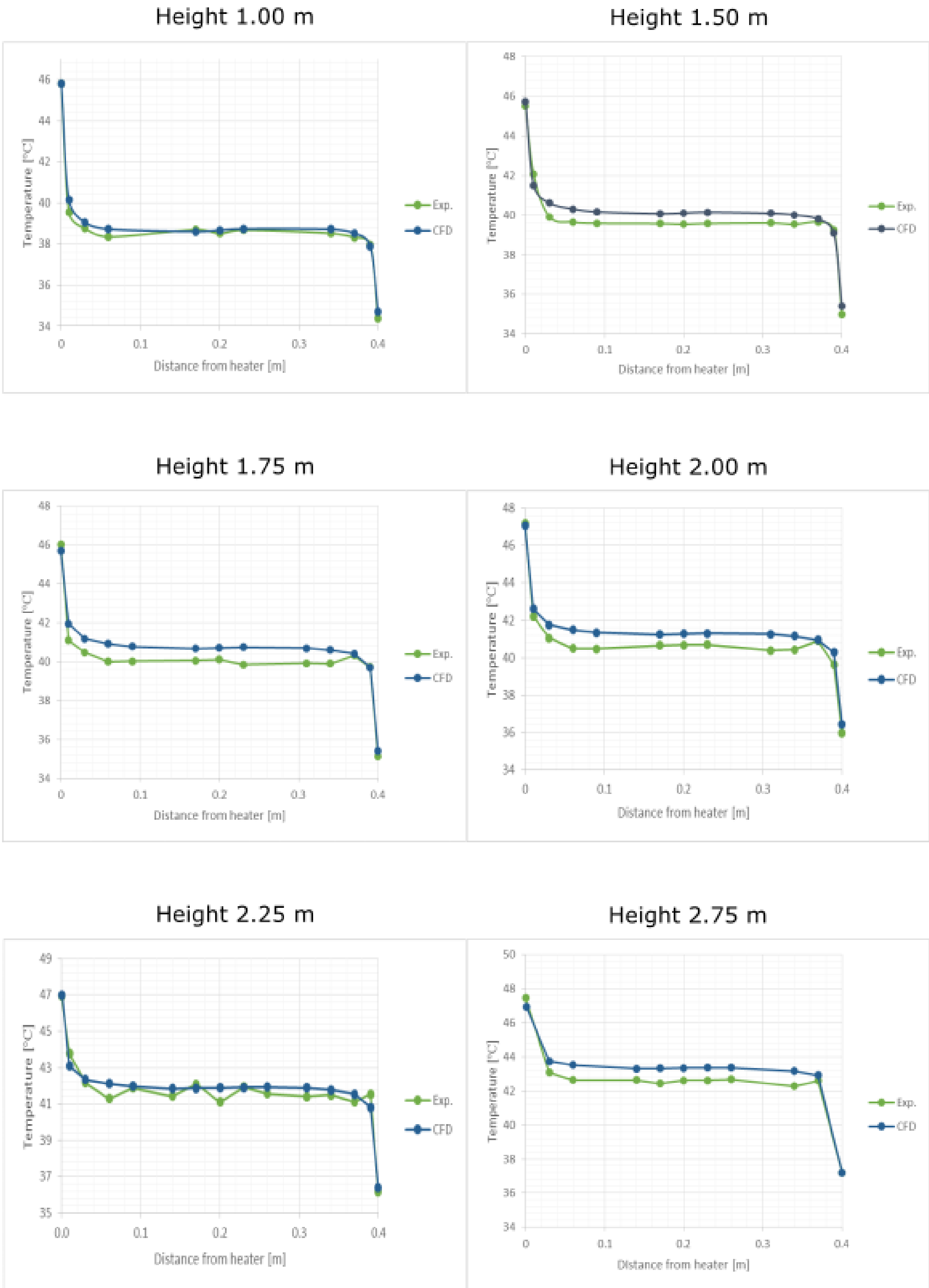

Figure 3.17. Experimental and analytical horizontal temperature profiles along the width of the cavity for different heights.

In general, the numerical and experimental temperature profiles had the same tendency. But the temperatures from the simulation with CFD were slightly higher than the measured one at about 0.5 °C. At the height of 2.25 m, the measured temperatures had fluctuations. This may happen because at this height was placed the most unstable heater with fluctuations up to 2.8 °C. Also there was a negative temperature gradient between the glass surface and the air inside the channel since the glass temperature was lower. Generally, due to the convection in the boundary layer higher temperature gradients exist near the walls. Outside the boundary layers, there is no temperature difference and the temperature profile is almost linear in the centre region of the flow. So it can be extracted from figure 3.17 at height 1.00 m that the boundary layer of heater and glass were expanded at a distance of 1 cm from the walls. As for the height of 1.50 m the heater boundary layer was higher than 1 cm and less than 3 cm, since there was no other measuring points between these distances to have a more clear view how the temperature was distributed between that points. For the same reason, the glass boundary layer was 1 cm or a little bit more. For both the height of 1.75 m and 2.00 m the boundary layer thickness for heater and glass was between 3 cm and 6 cm and at height of 2.75 m they were both bigger than 6 cm. In comparison with the calculated boundary layers in section 3.4 on page 15 they were found thinner.

3.6 Vertical Temperatures Profiles

The vertical temperature gradients were used to investigate the flow pattern and the development of the boundary layers. The dimensionless form of temperature was used to eliminate the effect of the measurements errors happened. For example an error occurred with the instability of the heaters which was mentioned in section 3.1. Therefore, for eliminating the influence of these instabilities the defined for each case set point for the heaters was chosen for the calculation of the dimensionless temperature. The influence of that error was observed for the vertical temperatures at the surface and at distance 1 cm from heaters and they were excluded. The same tendency happened as well for the temperature profiles of glass surface and at distance 1 cm because the glass was heated by radiation from the heaters according to the experimental set-up. The dimensionless vertical temperatures were calculated by the equation 3.2.

$$\frac{t_i - t_{SP}}{t_{out} - t_{SP}} \tag{3.2}$$

Where:

t_i	Measured temperature at point i
t_{SP}	Set point temperature used for the heaters
t_{out}	Measured temperature at the outlet

When the air was entering the channel, and it is not influencing by the boundary layer, is heated and it continues to warm along the height so its vertical temperature distribution will be linear and it will not change in the direction of the flow. This can be seen in figure 3.18 between the height of 0.25 m and 1.00 m. The vertical temperature profile at distance of 3 cm from the solid surfaces had a linear distribution, so it was not affected by the boundary layers, which were eliminated in smaller distance than 3 cm. After that height, it can be said that it met the boundary layers where there are higher temperature gradients. After the height of 1.75 m it continued to increase linearly as it happened at the beginning of its entrance into the channel and the flow did not be influenced by the boundary layers. This was an indication that either the flow was fully developed at that height or something else may happen. This would be investigated later. In a fully developed flow the fluid temperature does not remain constant. The fluid is heated and it continues to warm. So it will exist a generalized temperature distribution that it will not change in the direction of the flow as it could be observed here.

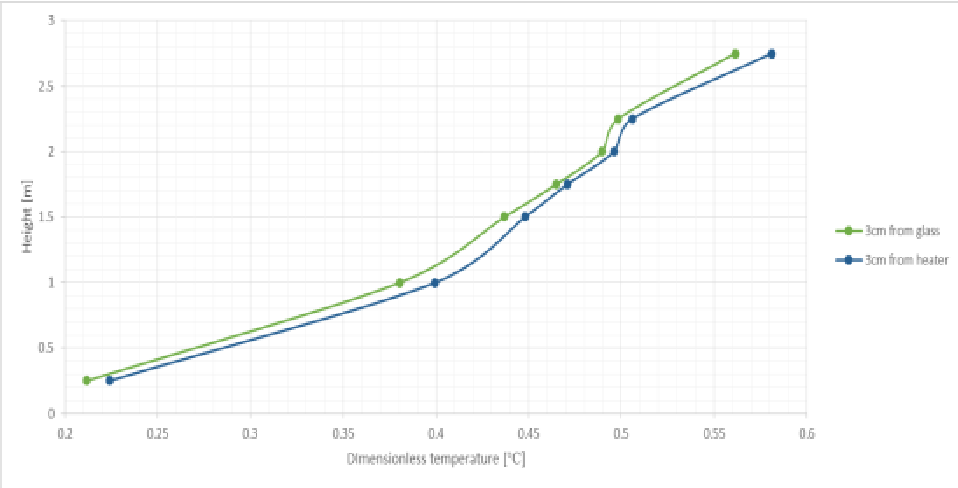

Figure 3.18. Vertical temperature gradients from surfaces at distance 3 cm.

In figure 3.19, the vertical gradient at distance of 6 cm met the thermal boundary layer at the height of 1.5 m.

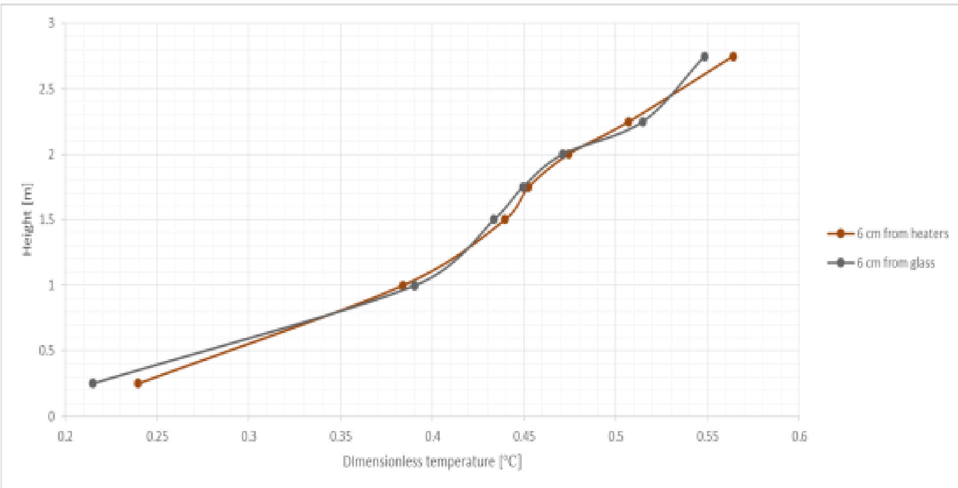

Figure 3.19. Vertical temperature gradients from surfaces at distance 6 cm.

The vertical temperature in thmiddle of the cavity which is presented in figure 3.20 was developing linearly along the height of the channel. Therefore, the flow in the middle of the cavity wase not affected by the development of the boundary layers.

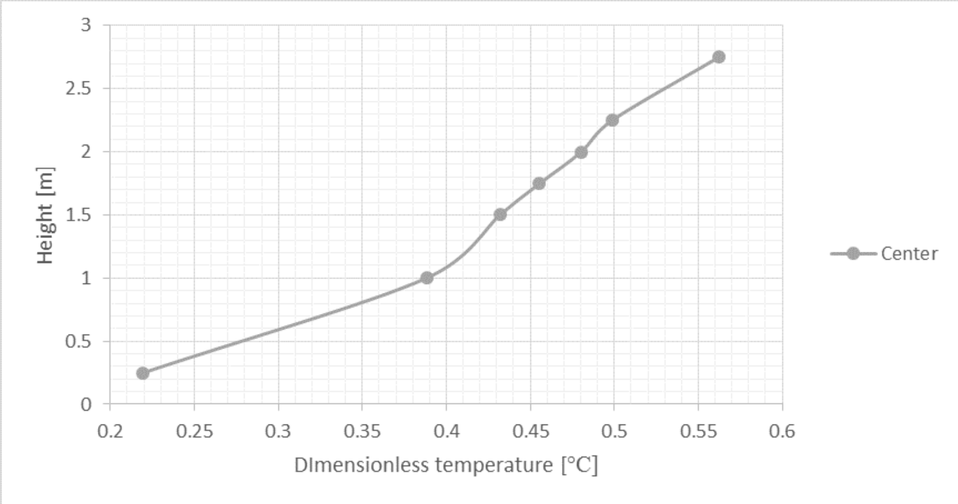

Figure 3.20. Vertical temperature gradients from surfaces in the center.

3.7 Velocity profiles

The experimental velocity measurements were conducted due to the time limit only for test number 12 with the usage of a Laser Doppler Anemometer as it was described in the Appendix A on page 35. A stability test for 300 seconds at a point in the channel which was located 1 cm from the glass surface at a height of 1.7 m was performed and it is shown in figure 3.21.

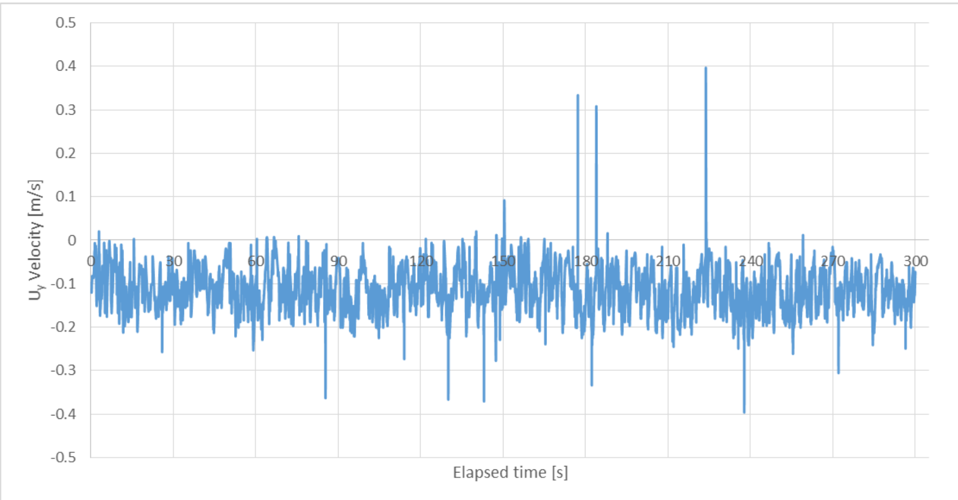

Figure 3.21. The time series of vertical velocities at height 1.75 m and distance 1 cm from glass.

The vertical velocity varied quickly between negative (down-flow) and positive (up-flow) values, the airflow was unstable. Therefore it was selected that the velocity at each measuring point to be represented of a mean value of 90 seconds. The velocities were measured at three different elevations and they were compared with the numerical solution in figure 3.22.

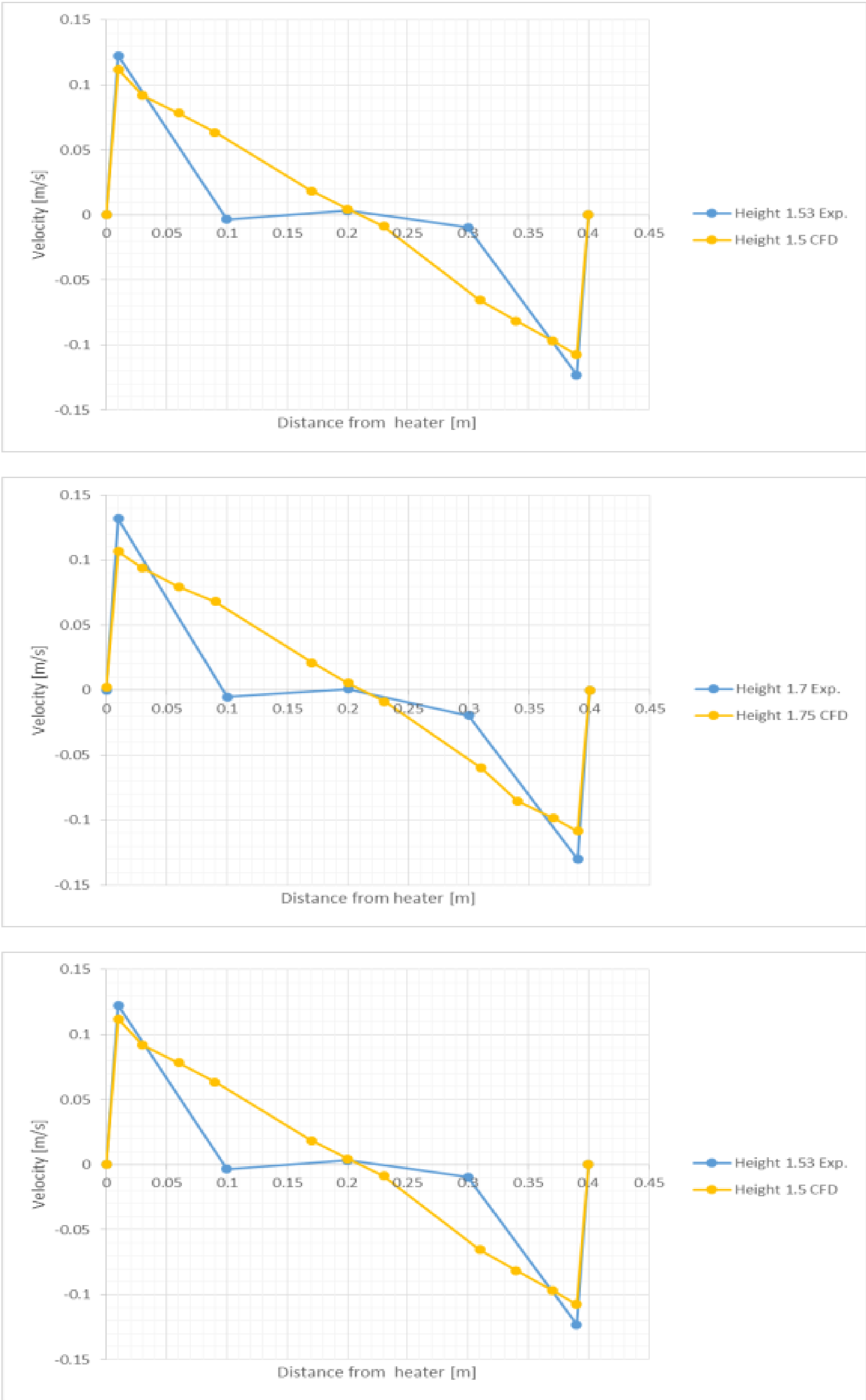

Figure 3.22. The numerical and experimental velocity profiles at three different heights for vertical channel.

Due to the fact that the Laser Doppler Anemometer measures in one direction and it measures the vertical U_y velocities, the velocities only in y-axis were taken for the comparison from the simulation.

In the experimental results for velocities the flow was eliminated at the boundary layers of the surfaces and there was almost no flow in the core region of the cavity. Due to the high surface temperatures and buoyant forces in the boundary layer, the velocity there, as it was expected to be, was higher than the air velocity in the main flow.

The case shows a circulation effect inside the cavity, with velocities with upwards direction at the region near the heater and downward direction at the region near the glass.

By integrating the velocity profiles from figure 3.22 the flow rate was found. The middle location of the channel at width of 0.20 m was almost symmetrical, with the air flow of 0.01 m^3/s distributed between the flow moving up at the heated wall and down at the glass wall at a percentage of 46% and 54 % respectively.
According to the analytical solution of the velocity profiles, the peak velocities in the boundary layers had only slightly differences but the velocities in the core region of the channel were different compared with the experimental velocities. The air flow rate was double than those of the experiment with a value of 0.02 m^3/s, which was distributed between the flow moving up at the heated wall and down at the glass wall at a percentage of 52% and 48% respectively.
In order to visualize this flow reversal the plot of the y velocities and velocity magnitude were illustrated in figure 3.23 and 3.24 respectively.

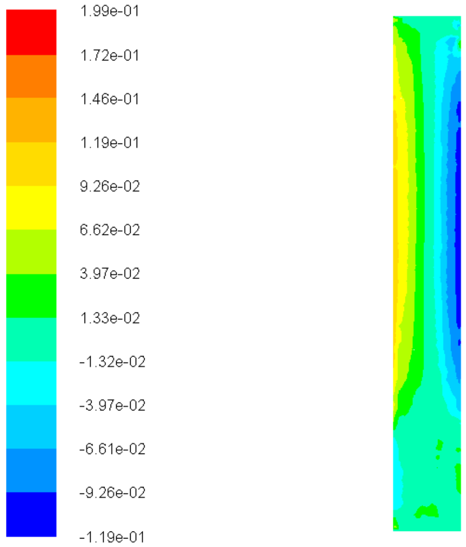

Figure 3.23. Contours plot of y velocity (in m/s).

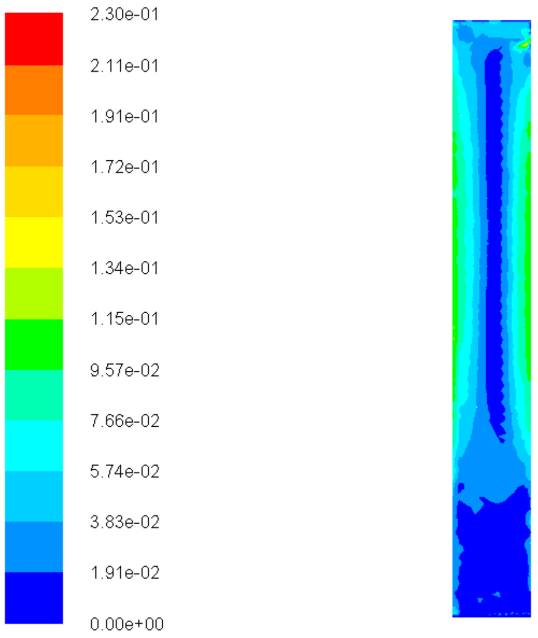

Figure 3.24. Contours plot of velocity magnitude (in m/s).

The flow was eliminated near the surfaces and the negative y-velocities happened at the glass surface. This extreme recirculation covered all the channel length and width. It had to be mentioned that the heater at the entrance level did not work and that was the reason that higher velocities due to buoyancy happened later and not from the beginning.

[Yilmaz, 2007] investigated numerically and experimentally the velocity and temperature field characteristic in a vertical channel. One channel wall was heated by a uniform heat flux and the other wall was adiabatic. Three Ra(b/L) values of 1.91×10^7, 2.74×10^7 and $\times10^7$ were used with an aspect ratio of 20. The numerical solution was carried out by using a Low Reynolds Number k-ϵ model. The model was capable of predicting the mean temperature field, but it grossly overestimated the velocity field especially in the core region of the channel.

Therefore, it can be said that the same happened in the test number 12. In that thesis, the analytical solution of temperature profiles for all the simulated cases had a good agreement with the experimental results but the velocity profiles had been overestimated in the core region of the channel.

CHAPTER

4 Numerical Investigation of Recirculation

The initial purpose of the experiment was the investigation of the recirculation flow, as it was explained by [Kalyanova, Olena] and it was written in the section 2 on page 5, in a vertical channel with one heated surface. For all the tested cases that were described in section 3.1 on page 9, it was observed that flow pattern for all the cases was almost similar. There was a recirculation effect in all the length of the channel, with velocities with upwards direction at the region near the heater and downward direction at the region near the glass. One explanation for this could be that the glass surface could not be heated enough by radiation from the heated surface and in all the cases the glass surface was in lower temperature than the air in the channel cavity. In order to investigate if that was the reason, a simulation of the cases number 7 and 12 were done with the usage of uniform temperature heating for the boundaries of both vertical surfaces. The characteristics of these cases could be seen in the section 3.1 on page 10. The applied temperature were taken from the experimental measurements. In this chapter the more representative case, which is case number 7 will be presented and the results of case number 12 could be found in electronic appandix C on page 51.

It is known in advance that the recirculation happens at the end of the channel and near the cooler surface [Kalyanova, Olena]. So, in that experiment set up, it was expected to take place near the glass surface which is influenced by the external environment due to its high thermal conductivity.

The velocity profiles will only presented without taking them into consideration. Because as it was concluded in section 3.7 on page 20, the numerical solution gives overestimated velocities especially in the core region which is in our interest since the recirculation happens when the flow rate enters the channel is not enough for further healthy development of the boundary layers. They are further developed in expense of the inviscid flow in the core region.
The thickness of the boundary layers of the surfaces was calculated according to the equation 3.1 on page 15 and are presented in figure 4.1. They were calculated to be 0.20 m for the heater and 0.19 m for the glass boundary layer. They were not merged at the last measuring height of 2.75 m and the flow was not fully developed but it was very close.

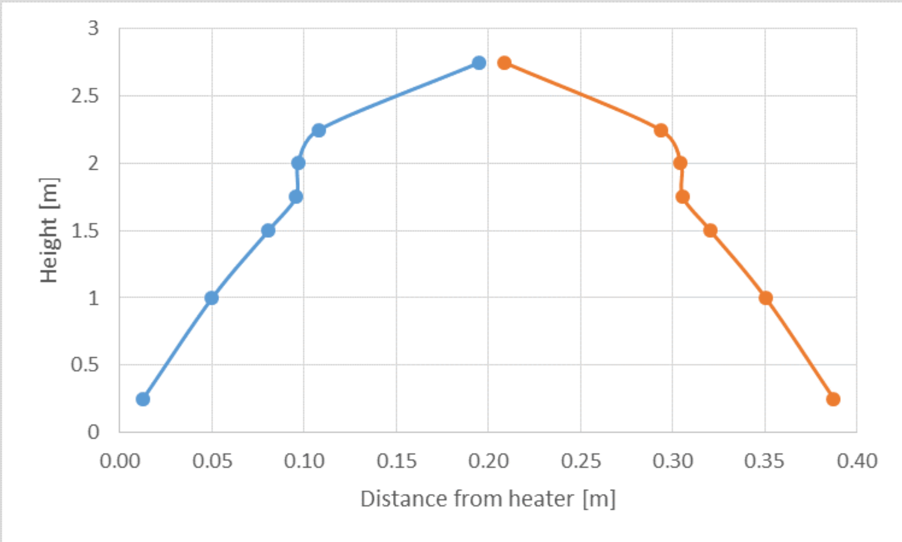

Figure 4.1. Thickness of boundary layers along the height.

To identify the flow regime, local Rayleigh numbers (both from glass and heater surface) were plotted in figure 4.2. They were calculated from the temperatures of the point i and from an average temperature of the surfaces. Negative Rayleigh numbers happened in the upper part where the fluid temperature was higher than the heater surface. All the others were in a range of 4.36×10^{10} to 1.03×10^{12}. According to [Incropera, Frank P, 2011] the transition to the turbulent flow happens at the critical Rayleigh number of 10^9, so the flow regime in that case was turbulent or in transition to turbulent flow regime

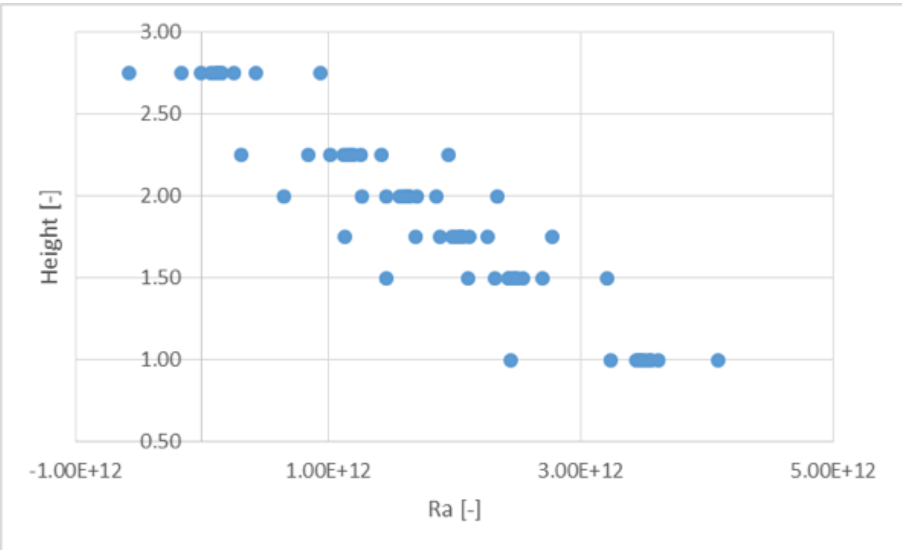

Figure 4.2. Local Rayleigh numbers from heater and glass surfaces.

The local Gr/Re^2 was calculated at the same way as the Rayleigh number from the equation 2.5 on page 6 in order to identify the convection regime. The convection regime was a free convection regime since it was dominated by the buoyancy forces. The highest values happened at the height of 0.25 m which is near the entrance plane.

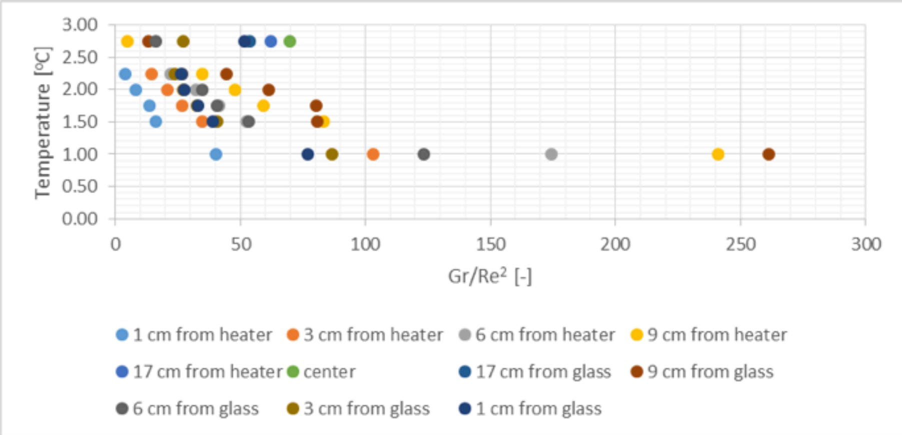

Figure 4.3. Identification of the convection regime.

The dimensionless vertical temperature profile at distances near the heater, the middle of the cavity and the glass are illustrated in figure 4.3. They were calculated at the same way as it was previously described in section 3.6 on page 18. From figure 4.4, the temperature gradients were linearly increased until the height of 1.00 m when they met the boundary layers where higher mixing of air happened and the temperature gradient decreased. The same tendency appeared as well in figure 4.5 with the only difference that vertical gradients met the boundary layer at the height of 1.50 m.

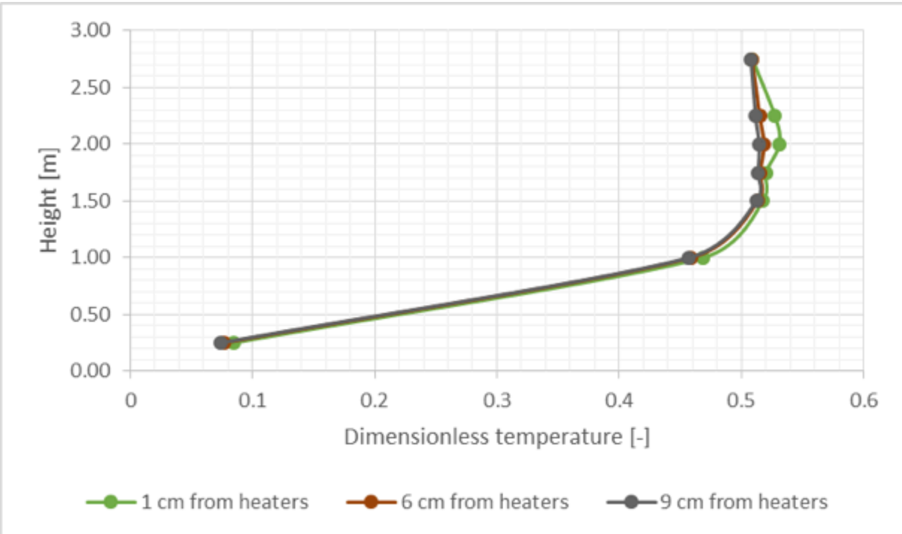

Figure 4.4. Vertical temperature gradients at distances from heater.

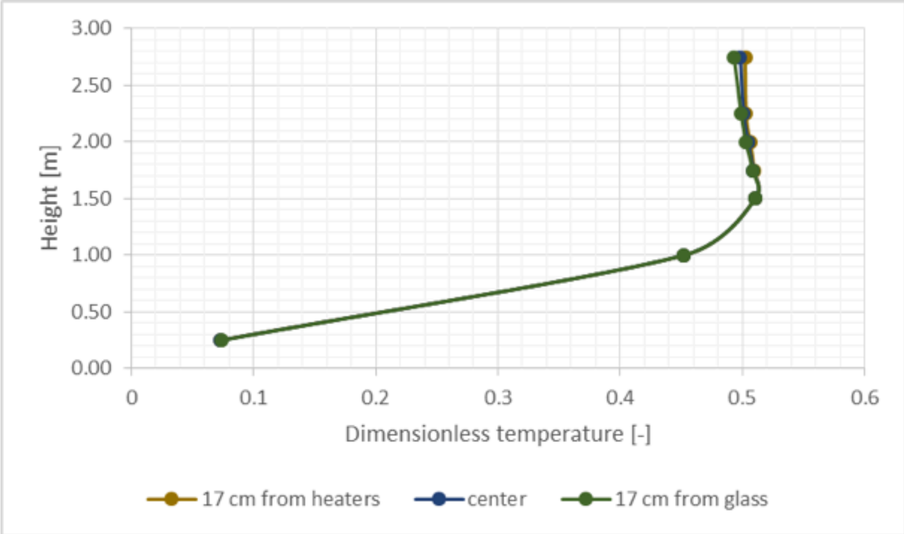

Figure 4.5. Vertical temperature gradients at the centre of the channel.

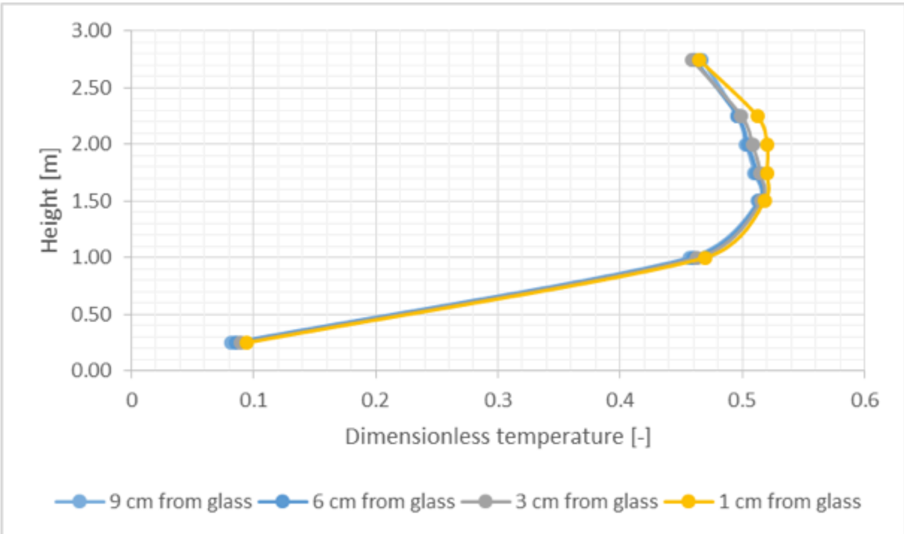

Figure 4.6. Vertical temperature gradients at distances from glass.

In figure 4.6 for the vertical gradients near the glass, it was observed deformation of temperature profiles from the height of 1.5 m at distances 3, 6, 9 cm from glass and the maximum air temperatures appeared not at the top of the channel but lower which can be caused by recirculation. The local Gr/Re^2, between the heights 1.50-2.75 m had a ratio up to 80.

The velocity profiles from the numerical solution is presented in figure 4.7. The velocity magnitude, which is the sum of the absolute values of the three velocity vectors (x,y,z), was used for the plot of the velocities. According to figure the flow is fully developed after the height of 1.75 where there were no maximum peak velocities in the boundary layers and the velocity was almost distributed in a uniform way along the cavity of the channel. The velocity profile at the height of 2.75 m might be influenced by the outlet. But, if the fact that the velocities according to [Yilmaz, 2007] were overestimated in the core region of the channel, was taken into consideration, it can be assumed that the flow was not fully developed yet but in a transitional phase. But it is only an assumption and further experimental investigation for the velocities is needed to be done. From the numerical solution of velocities, only the maximum velocities at the bounder layers could be taken into consideration.

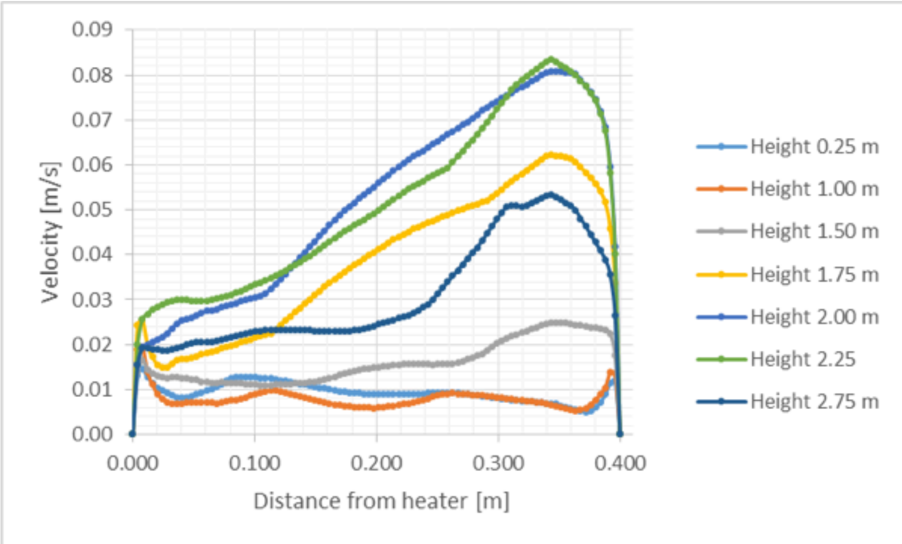

Figure 4.7. Velocity profiles in the vertical channel.

The static temperature and velocity distribution of the flow in the cavity is visualised in figures 4.8 and 4.9. In an area near the glass surface and above the half length of the channel, it is observed lower distribution of temperatures and higher velocity. It is an indication of recirculation since in the recirculation area happen higher velocities and higher mixing of air between boundary layer and main flow.

Moreover, according to the vertical temperature gradients in figure4.6 the penetration of this recirculated area was expanded until the distance of 9 cm from the glass surface since vertical temperature gradients were not created for bigger distances from the glass until the middle of the cavity so it was not clear until which distance from the glass the recirculation took place. But from the contour plot of the temperatures, it can be seen that the area with higher velocities and air mixing was expanded almost until the middle of the cavity.

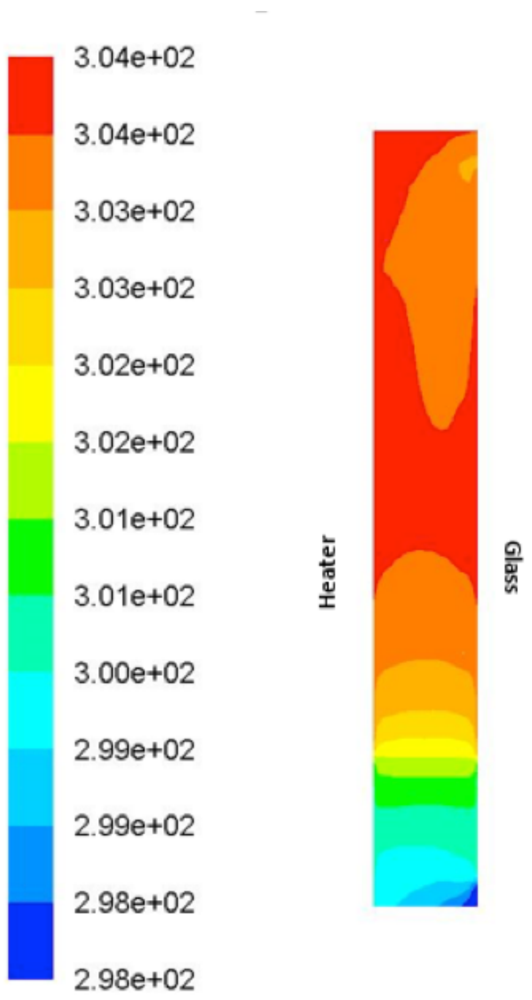

Figure 4.8. Contours of static temperature (in K).

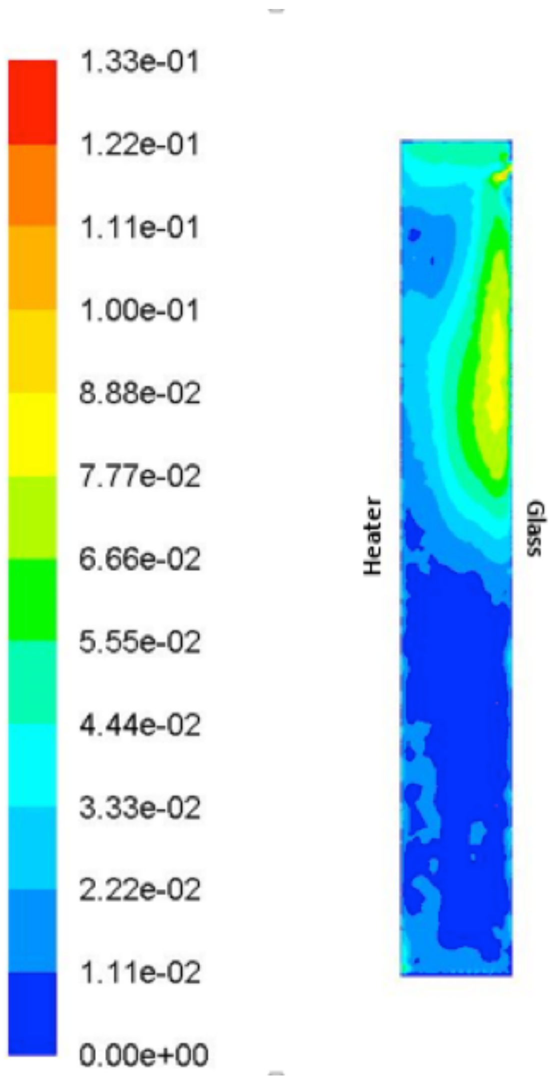

Figure 4.9. Contours of velocity magnitude (in m/s).

At this chapter an effort was performed in order to investigate further if the recirculation in the cavity was possible to happen. During all the experiments, the glass surface was not heated enough and an extreme flow reversal was happening along the whole height of the vertical channel for all the cases.

To identify if that was the error of the flow reversal phenomenon, a simulation was performed with the usage of uniform temperature boundary conditions for both surfaces and it was proved that the flow developed as it was expected and the recirculation phenomenon took place. Therefore it can be concluded that previously stated problem with the glass surface temperature prevented the recirculation of being happened.

CHAPTER

5 Conclusion

The objective of this project was to investigate the air flow pattern in vertical channel with heated surface. In literature there are not so many studies about the transitional flow regime that happened between the laminar and turbulent flow. An application of vertical heated channels is at the Double Skin Façade used in buildings and according to [Kalyanova, Olena] there was an indication of recirculation in the cavity that may be happened in the transitional regime. To confirm this indication, experimental measurements were carried out in a vertical channel with an aspect ratio of 1/8 (width/length). According to the experimental set up the one of the vertical surface would be heated by conduction from electrical heating mats and the other surface which was made of glass in order to resemble a double skin façade was heated by radiation. This surface had a high thermal conductivity and it was influenced by the ambient conditions in the laboratory facility. Thirteen different cases were tested with a range of Rayleigh number of 3.3×10^{12} to 12.0×10^{12}. The cases were grouped according to some main characteristics such as the ACH and the heat input. For the majority of the cases, uniform temperature at the heated surface was used. Horizontal and vertical profiles were created in order to see the temperature distribution and the development of thermal boundary layers of both surfaces along the height. Their thickness was calculated and velocity profiles were presented as well. The experimental results were compared with the numerical solution, which was obtained by a CFD simulation created by the software of Ansys Fluent. By comparison of them it was extracted that the temperature results from the simulation model had a good agreement with the measured temperatures during the experiments. On the contrary, as for the comparison of velocities it was found that the CFD model was capable of finding the peak velocities at the boundary layers but the velocities in the middle core region of the channel were overestimated. For all the tested cases the temperature of the glass surface was lower than the fluid temperature in the cavity. In all cases, a flow reversal which was moving upwards from the heated surface and moving downwards from the glass surface was observed. The penetration of this reversal flow covered almost all the length of the vertical channel. Due to that, it was not able to create the appropriate thermal conditions and a healthy development of the boundary layers in order to be able for the recirculation to happen. The indication was that the glass surface was not heated so much. In order to identify this a CFD simulation were performed by using uniform temperature boundary conditions for the test case number 7 and 12. Only the temperature results were taken into consideration since it was proved before that the numerical solution overestimated the velocities in the core region of the cavity which is the region that was expected the recirculation to happen. From the vertical temperature gradients it was observed a deformation of the temperature profiles and the higher temperatures did not happen at the top of the channel but at the lower height of 1.50 m and at distances of 9 cm from the glass surfaces. (Vertical temperature gradients were not created for bigger distances from the glass so it was not clear until which distance from the glass the recirculation took place).

5.1 Future Work

The CFD-simulation of the channel flow in which the recirculation happened could be used as a benchmark in future work in the test facility in the laboratory in order to create the appropriate thermal conditions that are needed to obtain the transitional flow regime and to catch the recirculation. It can be also used to optimise the airflow in the cavity.
Moreover, what has to be done in the experimental facility in order to get rid of the flow reversal in the whole cavity is to increase the temperature at the glass surface. This can be done either by reducing the cavity width in order to heat the glass surface more by the radiation or by thermal insulating the glass.

Bibliography

Alzwayi, Ali Saad, **2013**. Alzwayi, Ali Saad. *Transition of free convection boundary layer flow*, 2013.

Artmann, Nikolai and Vonbank, R and Jensen, Rasmus Lund, **2008**. Artmann, Nikolai and Vonbank, R and Jensen, Rasmus Lund. *Temperature measurements using type K thermocouples and the Fluke Helios Plus 2287A Datalogger*, Department of Civil Engineering, Aalborg University, 2008.

Ayinde, **2008**. Ayinde. *Turbulent natural convection flow in a vertical channel with anti-symmetric heating.* Heat and Mass Transfer, 44(10), 1207–1216, 2008.

Bacharoudis, Evangellos, **2007**. Bacharoudis, Evangellos. *Study of the natural convection phenomena inside a wall solar chimney with one wall adiabatic and one wall under a heat flux.* Applied Thermal Engineering, 27(13), 2266–2275, 2007.

Badr, HM and Habib, **2006**. Badr, HM and Habib. *Turbulent natural convection in vertical parallel-plate channels.* Heat and mass transfer, 43(1), 73–84, 2006.

Baldinelli, G, **2009**. Baldinelli, G. *Double skin façades for warm climate regions: Analysis of a solution with an integrated movable shading system.* Building and Environment, 44(6), 1107–1118, 2009.

Dantec Dynamics. Dantec Dynamics. *Measurement principles of LDA.* URL: `http://www.dantecdynamics.com/measurement-principles-of-lda`. Downloadet: 04-6-2015.

Davies, Morris Grenfell, **2004**. Davies, Morris Grenfell. *Building heat transfer.* John Wiley and Sons, 2004.

Eckert, ER and Jackson, Thomas W, **1950**. Eckert, ER and Jackson, Thomas W. *Analysis of turbulent free-convection boundary layer on flat plate*, DTIC Document, 1950.

Gau, C and Yih, KA and Aung, Win, **1992**. Gau, C and Yih, KA and Aung, Win. *Measurements of heat transfer and flow structure in heated vertical channels.* Journal of thermophysics and heat transfer, 6(4), 707–712, 1992.

Heiselberg, Per and Sandberg, Mats, **1990**. Heiselberg, Per and Sandberg, Mats. *Convection from a slender cylinder in a ventilated room*, Dept. of Building Technology and Structural Engineering, 1990.

Incropera, Frank P, **2011**. Incropera, Frank P. *Fundamentals of heat and mass transfer.* John Wiley and Sons, 2011.

Jiru, Teshome Edae and Tao, Yong-X and Haghighat, Fariborz, **2011**. Jiru, Teshome Edae and Tao, Yong-X and Haghighat, Fariborz. *Airflow and heat transfer in double skin facades.* Energy and Buildings, 43(10), 2760–2766, 2011.

Kalyanova, Olena. Kalyanova, Olena. *Double-Skin Facade: Modelling and Experimental Investigations of Thermal Performance.*

Michael Andersen, **2014**. Michael Andersen. *TheProcessOfHeatTransfer.* URL: `http://www.einsten.net/10/2014/10/processen-med-varmeoverforsel.html`, 2014. Downloadet: 04-6-2015.

Miyamoto, **1982**. Miyamoto. *Development of Turbulent characteristics in a vertical free convection boundary layer.* 7th International Heat Transfer Conference, pages 323–328, 1982.

Pasut, Wilmer and De Carli, Michele, **2012**. Pasut, Wilmer and De Carli, Michele. *Evaluation of various CFD modelling strategies in predicting airflow and temperature in a naturally ventilated double skin façade.* Applied Thermal Engineering, 37, 267–274, 2012.

Safer, Nassim and Woloszyn, Monika and Roux, Jean Jacques, **2005**. Safer, Nassim and Woloszyn, Monika and Roux, Jean Jacques. *Three-dimensional simulation with a CFD tool of the airflow phenomena in single floor double-skin facade equipped with a venetian blind.* Solar Energy, 79(2), 193–203, 2005.

Schlichting, Herrmann and Gersten, Klaus and Gersten, Klaus, **2000**. Schlichting, Herrmann and Gersten, Klaus and Gersten, Klaus. *Boundary-layer theory.* Springer Science and Business Media, 2000.

Wirtz, RA and Stutzman, RJ, **1982**. Wirtz, RA and Stutzman, RJ. *Experiments on free convection between vertical plates with symmetric heating.* Journal of Heat Transfer, 104(3), 501–507, 1982.

Yilmaz, **2007**. Yilmaz. *Temperature and velocity field characteristics of turbulent natural convection in a vertical parallel-plate channel with asymmetric heating.* Heat and mass transfer, 43(7), 707–719, 2007.

APPENDIX

A Introduction to experiment

A.1 Equipment list

The following equipment was used in the experimental setup for the vertical channel with one heated surface:

- PC with LabView
- Carawarm heating mats
- Thin type K thermocouples
- Fluke Helios Plus 2287A data logger
- Compensation box
- Ice point reference KAYE K170-6
- Exhaust fan
- Power transducer
- Smoke machine with controller
- Two Dantec Laser Doppler Anemometer
- PC's with BSA flow software
- Mechanical traverse system for LDA

A.2 Description of the Experimental Set-up

For the experimental investigation of the air flow pattern in a vertical channel, a test apparatus of a single box window was designed and constructed in the klima-laboratory at Aalborg University to resemble and represent the smallest subunit of all the double skin façade systems.

The main dimensions of the apparatus were length x height: 1.55 m x 3.03 m. The facility had been constructed in such a way that allowed the adjustment of the cavity width in a range between 0.05 m and 0.50 m. In order to limit the heat transfer between the test facility and its surroundings, it had been enhanced by 100 mm EPS, which was enclosed by 12 mm of plywood. The facility can be seen in figure A.1 and A.2 on the following page.

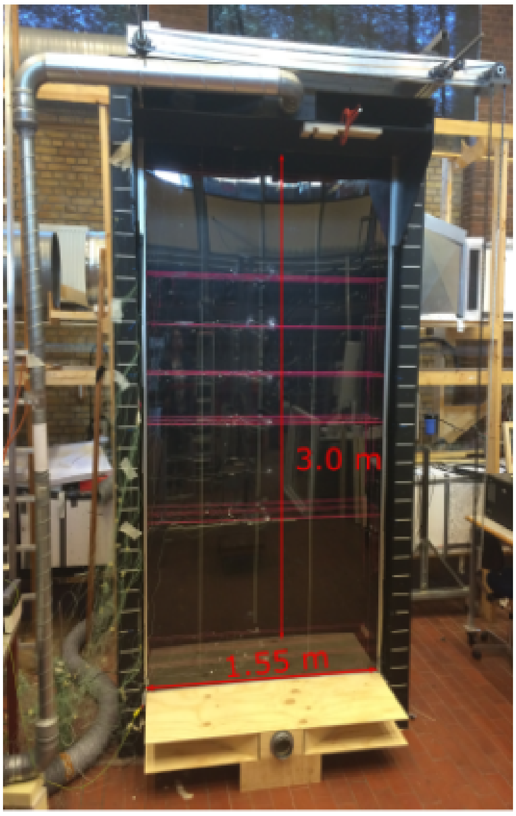

Figure A.1. Photo of the laboratory test facility.

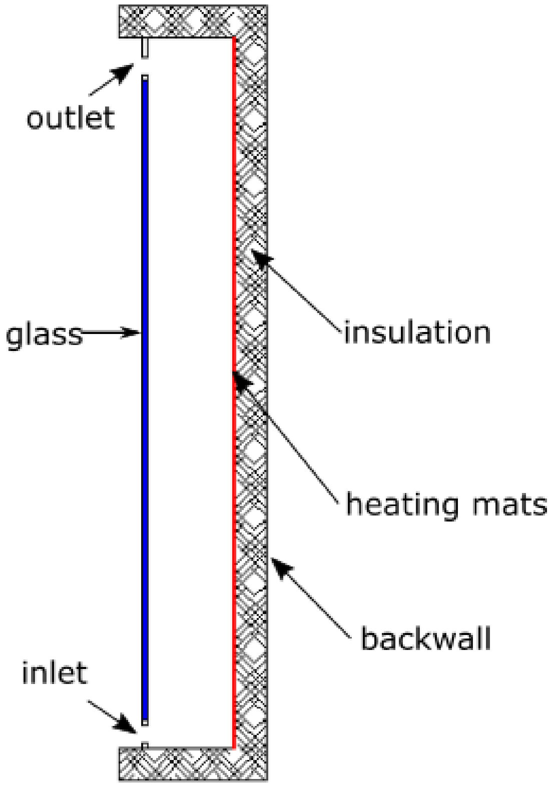

Figure A.2. Sketch of the test facility of the vertical channel.

The front glass surface was 2.73 m high and 1.55 m wide compromising an aluminium frame of 0.025 m. It was made of 3 mm polycarbonate plastic with a density of 1.20 g/cm^3, and its thermal conductivity was 0.21 W/m · K.

The inlet was designed at the bottom and the outlet at the top of the glass surface, with an area of 0.105 m^2 for both of them. For the constructed apparatus the inlet air was set to be the ambient air of the laboratory. The outlet was controlled by a fan equipped with an orifice plate to regulate the flow rate at the exit. This choice of the outlet and inlet were done with respect to the lesser possible influence of the flow inside the cavity from external factors, since the idea of the set up was to investigate the buoyancy effect resulting in air recirculation for different widths and heat inputs in a vertical channel.Due to the mass balance of the box and with the assumption of air tight construction, it was assumed that the flow rate exiting the test facility was the same as the flow rate entering. So, in that way the inlet flow rate was known in advance and could be adjusted.

For having the heat input gradually or uniformly distributed into the cavity, five electrical heating mats made from Carawarm foils were placed into the back wall (insulated wooden plate). Each electrical heating mat consisted of a maze of hot wires, with an area of 600 mm x 1500 mm and a power of 480 W. Their temperature can be controlled and modulated manually and separately for each one of the five heating mats. By this way, a temperature gradient could be obtained with a maximum of 15 °C difference. Their construction and the way they were placed into wooden back wall is presented in figure A.3.

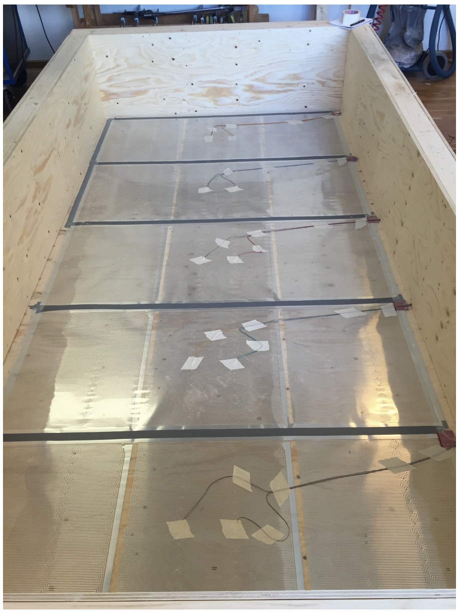

Figure A.3. Placement of the electrical heating mats into the backwall of vertical channel.

A.2.1 Temperature measurements

The measurements of the temperature inside the tested cavity were conducted by using thin thermocouples type K for both surfaces and air measurements. 89 measuring locations for a 40 cm cavity were used distributed on different heights and on different positions in each height. The location of the thermocouples can be found in figure A.4.The thermocouples on the surfaces were located above thermal paste in order to have good contact with the surface. The material has a high thermal conductivity and will therefore transfer the heat to the thermocouple.

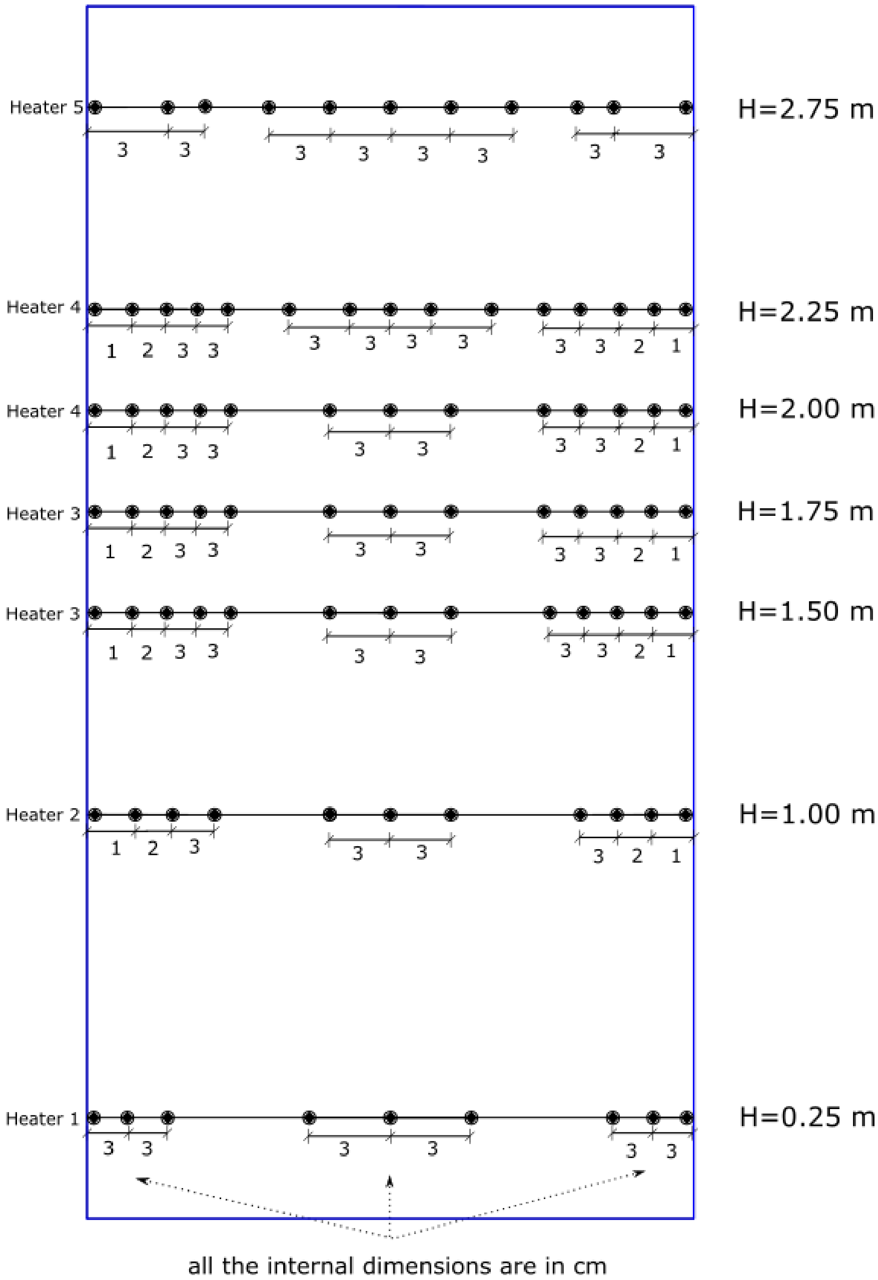

Figure A.4. Position of the thermocouples in the vertical channel.

For higher precision in temperature measurements, the thermocouples were calibrated at reference temperatures in ten steps going from 10 °C to 50 °C. The temperatures were

registered every 9 seconds by a Helios data logger which was connected to a KAYE K170-6 ice point reference. All the thermocouples were connected in an isolated compensation box and protected from the ambient conditions, to increase the accuracy of the measurements. The total uncertainty of the temperature measurements for thin thermocouples was calculated to be 0.086 K, without taking into account the impact of the radiation from the surrounding surfaces as it is referred by [Artmann, Nikolai and Vonbank, R and Jensen, Rasmus Lund, 2008] for the usage of the same equipment for the thermocouples.
Finally, for preventing the noise in the electrical signals of the thermocouples, all the used devices were properly grounded. By grounding, the electric noise was reduced to ± 0.1 K.

A.2.2 Velocity Measurements

The following section is based on [Dantec Dynamics].

An 1D type of Laser Doppler Anemometer (LDA) which was equipped with a burst spectrum analyzer (BSA) was used to measure the air velocity in the vertical channel. The LDA is an optical non-intrusive instrument that measures the particle flow in gases and fluids. The principle of the LDA is shown in figure A.5. It consists of a continuous wave laser, transmitting optics including a beam splitter and a focusing lens, receiving optics as a focusing lens, an interference filter and a photodetector, and at last a signal processer.

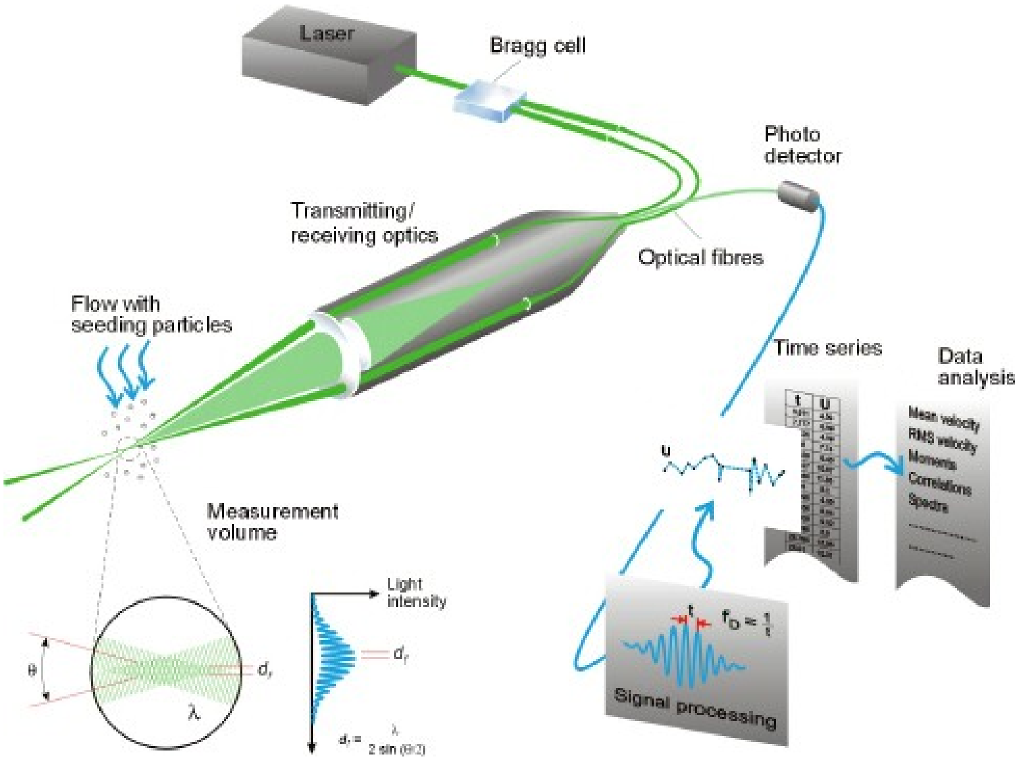

Figure A.5. LDA principle. [Dantec Dynamics]

As the figure is showing a brag cell is used as the beam splitter that creates vibrations, which generate acoustical waves acting like an optical grid. From this, two laser beams are produced with equally intensity but different frequencies. The laser beams are brought to the probe, where after the lens force them to intersect in a probe volume, the measurement volume showed in figure A.5 and this volume is only a few millimeters long. Fringes, which are parallel planes of high light intensity, are created in the measurement volume due to interference between the two laser beams. When seeding particles pass this area the scattered light contains a Doppler shift, the Doppler frequency, which is proportional to the velocity measured perpendicular to the probe volume. The scattered light is then send back to the lens and focused on a photo-detector, that analysis the light intensity according to frequency and speed of the particle, since velocity equals distance divided by time.

The locations where the LDA probes conducts the velocity measurements has to be known with high accuracy. For that reason a 2D traverse mechanism were used to know the coordinates with high accuracy.

Fog droplets generator was used to create particles that can be traced by the LDA. It was needed to take into consideration that the smoke machine warms the incoming air, so the smoked air entered into the cavity was warmer than the ambient air. For that reason, the smoke was streamed into a 1 m long tube to ensure that the smoke, after it was generated and before entering the cavity, was cooled off and resembled the ambient air.

The inlet of the cavity was a free ambient air inlet, and the air temperature could vary according to the ambient conditions. For that reason, in order to reduce this uncertainties and to have the almost same ambient conditions during the measurementsas, the measurements were performed by using two DANTEC Flow LDA laser probes . The first laser was positioned steady in the middle of the cavity at the height of 1.20 m from the inlet height and the second was placed on the traverse mechanism and measured the velocities for different locations as it is illustrated in figureA.6. Only measurements from the second laser were used when the first laser with constant location showed a nearly steady state.

Also, it has to be mentioned that the laser, which was located steadily had a lens suitable for measuring distances up to 160 mm and the second one located on the traverse system had a lens that measured distances up to 400 mm. For each measuring point, the readings of 89 thermocouples were taken. The purpose of these readings was to compare the effect of adding smoke to the measurements conducted without smoke.

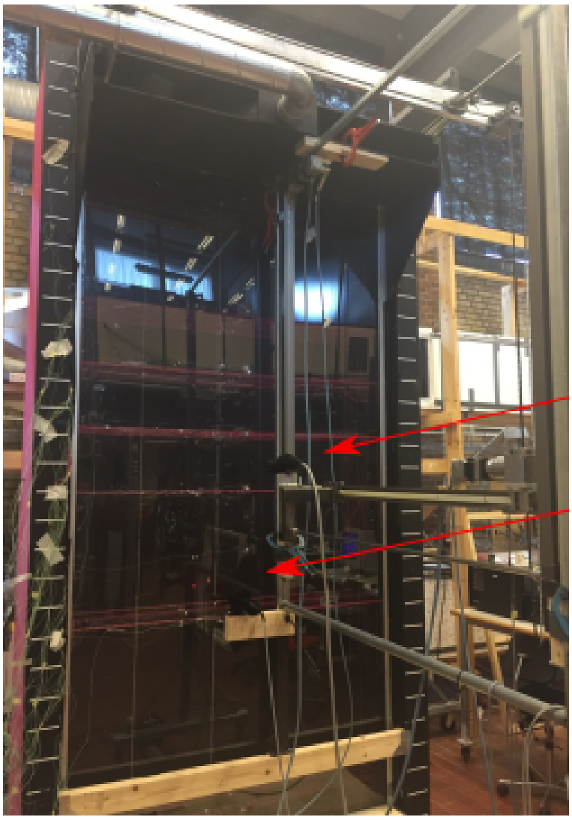

Figure A.6. Position of two lasers for velocity measurements.

To ensure that the first measuring position of the laser probe was in accordance with the measuring location of the thermocouple, the probe was traversed towards the heating wall, and it was assumed that it was coincident with the wall surface when the signal amplitude of the probe was at maximum [Yilmaz, 2007]. From that point, the laser probe was moved to the first wanted location.

The results of the velocity measurement are presented and analysed in 3.7 on page 20.

APPENDIX

B Numerical solution of the airflow in vertical channel by using CFD

The knowledge of the airflow pattern and the air temperature distribution in vertical channel is of a great importance in order to evaluate its thermal performance. This can be achieved by three different model techniques: the physical model that it is used for having an experimental solution, the mathematical model that gives an analytical solution and the computational model that provides a numerical solution. The computational models use finite element method approximations and provide solutions for each grid point of the domain, both in space and time.

In this chapter the airflow and the heat transfer phenomena of a vertical channel will be modelled and simulated by using numerical simulation derived by the use of a CFD software programme (Fluent by Ansys).

B.1 Geometry Model

The geometry model of the channel is based to the one used during the experimental study and it was described in Appendix A.2 on page 35. The inlet was set at the bottom of the glass surface and the outlet at the top. Both of them they have an area of $0.105\,m^2$. The geometry and the mesh were created by using the software of ICEM. The model geometry is presented in figure B.1 on the next page.

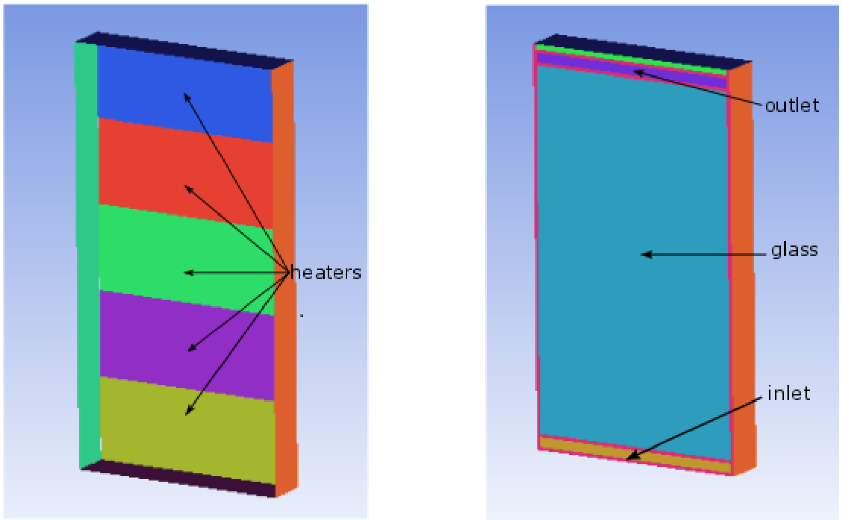

Figure B.1. The geometry model of the test facility.

B.2 Mesh features and grid independency

The first thing that has to be done before a CFD analysis is the grid generation for the whole domain of interest. For the mesh generation of the model, it was selected to use unstructured patch independent mesh with triangular shapes for the surfaces, tetrahedral for the volume and prism layers near the boundaries. The main advantage of the unstructured mesh is that the mesh can be refined in an easy way in regions where large flow gradients occur, such as the inlet, the outlet, near wall regions etc. The boundary layers in free convection play an important role because the solution gradients in that area are very high. To capture the phenomenon of convection, it should be used a fine mesh but that has as a drawback at time and convergence. Instead, adding prism layers near the walls would be a time and cost effective solution.
Additionally, a grid independency test was done for a number of mesh sizes in order to ensure that the solution is independent of the grid size. So, a grid of 350.332 cells was selected.

B.3 General decisions

Due to uncertainty about the phenomenon of the airflow recirculation, whether it happens or not, the steady state simulation was chosen with respect to the computational time and to the criterion of easier convergence.
The gravity exists in the y-axis of the geometry model and the pressure based solver was chosen for a low speed incompressible flow as it happens for the fluid in the channel.

B.4 Properties of the fluid material

The fluid was chosen to be the air. As for its density, the Boussinesq approximation, given by the equation B.1 had been used.

$$\rho = \rho_0(1 - \beta\Delta T) \tag{B.1}$$

Where:

ρ_0	Constant density of the flow [kg/m^3]
β	Thermal expansion coefficient [k^{-1}]
ΔT	Temperature difference [K]

According to Boussinesq approximation, the density differences can be neglected for small temperature gradient, so the density can be treated as a constant value in all the solved equations, except for the buoyancy term in the momentum equation. This density treatment is considered sufficiently accurate as long as the changes in density are small like it happens in indoor airflows.

The others air properties of the air such as the thermal conductivity λ [Wm^{-1}K^{-1}] and the specific heat capacity C_p [Jkg^{-1}K^{-1}] were treated as constant values because according to [Pasut, Wilmer and De Carli, Michele, 2012], it is not worthy to treat these values as a function of the density. This treatment increases the computational time without any significant improvement of CFD prediction . The changes of λ and C_p are only 2.6 % and 0.1 % respectively at temperature of 293.15 K.

B.5 Airflow equations

The airflow in the cavity is the result of free convection, therefore it is driven by buoyancy forces. It can be described by the equations of mass, energy and momentum conservation, together with the definition of the turbulent flow variables [Baldinelli, G, 2009]. The general form of the governing equations is shown in equation B.2.

$$\frac{\partial(\rho\phi)}{\partial t} + div(\rho\vec{U}\phi) = div(\Gamma_\phi grad\phi) + S_\phi \tag{B.2}$$

Where t is the time, ρ is the air density, $\vec{U}$ is the velocity vector, Γ_ϕ is the diffusion coefficient, S_ϕ is the source term of the general form where ϕ can be the temperature T, the velocity components u, v, w, the turbulent kinetic energy k or the dissipation rate ϵ.

B.6 Modelling the Turbulence

The aim of the simulation was to find the air recirculation in the cavity of the DSF, although there is uncertainty about its existence. From the measurements conducted in a DSF by [Kalyanova, Olena], the flow regime in the cavity, according to the measured velocity profiles showed that the flow was not fully developed turbulent when the recirculation happened. The right choice of a turbulence modelling method is of a great importance since it ensures the accuracy of the model.

B.6.1 Turbulent Model

Therefore, for the simulation of the vertical channel the k-ϵ realizable model was selected. It is suitable for a wide range of flows, such as the channel flow and layer flow. Moreover, it has good performance for flows involving rotation, boundary layers under strong adverse pressure gradients, separation and recirculation [Safer, Nassim and Woloszyn, Monika and Roux, Jean Jacques, 2005]. Moreover, the chosen turbulence model, except the turbulence flow, is able to deal with the laminar and the transitional flow.

In general, the k-ϵ model is a two equations Reynolds averaged Navier-Stokes based model. It uses two more transport equations for the kinetic energy k and the dissipation rate ϵ. These equations are presented in B.3 and B.4.

$$\frac{\partial}{\partial t}(\rho k) + \frac{\partial}{\partial x_j}(\rho k u_j) = \frac{\partial}{\partial x_i}\left[\left(\mu + \frac{\mu_t}{\sigma_k}\right)\right]\frac{\partial k}{\partial x_j} + G_k + G_b - \rho_{\epsilon\epsilon} - Y_M + S_k \tag{B.3}$$

$$\frac{\partial}{\partial t}(\rho \epsilon) + \frac{\partial}{\partial x_j}(\rho \epsilon u_j) = \frac{\partial}{\partial x_j}\left[\left(\mu + \frac{\mu_t}{\sigma_\epsilon}\right)\frac{\partial k}{\partial x_j}\right] + \rho C_1 S_\epsilon - \rho C_2 \frac{\epsilon^2}{k + \sqrt{\nu\epsilon}} + C_{1\epsilon}\frac{\epsilon}{k} + C_{3\epsilon} G_b + S_\epsilon \tag{B.4}$$

Where:

k	Turbulent kinetic energy
ϵ	Dissipation rate
G_k	Generation of turbulent kinetic energy due to the mean velocity gradients
G_b	Generation of turbulent kinetic energy due to the buoyancy
Y_M	Contribution of the fluctuating dilatation in compressible turbulence to the overall dissipation rate
S_ϵ	Source term
$\sigma_k - \sigma_\epsilon$	Turbulent Prandtl numbers for k and ϵ

The eddy viscosity is calculated from equation B.5.

$$\mu_t = \rho C_\mu \frac{k^2}{\epsilon} \tag{B.5}$$

Where μ_t is the turbulent viscosity, ρ is the density, C_μ is a term that it will be calculated for the realizable k-epsilon model and it is not constant like the other k-epsilon models, k is the kinetic energy and ϵ is the dissipation rate. The values of the model constants are given in Table B.1. These default values have been arrived at by data fitting for a wide range of turbulent flows.

$C_{1\epsilon}$	C_2	σ_κ	σ_ϵ
1.44	1.9	1.0	1.2

Table B.1. The constants values in the k-ϵ realizable model.

B.6.2 Near-wall Treatment

For the near wall region in the k-ϵ model, the standard wall function was used. The choice of the wall treatment depends on the non-dimensionless distance value y^+ from the wall to the first node of the mesh. The standard wall function implies that our near wall cells lies completely in the logarithmic region of the boundary layer. It corresponds to the region where the turbulent shear stress is dominant.

B.7 Radiation Model

The thermal radiation heat transfer between the surfaces was calculated by making use of the *surface-to-surface* radiation model, since the model is appropriate for enclosure radiative heat transfer. The model assumes all surfaces to be grey and diffuse. Emissivity and absorption of a grey surface are independent of wavelength. By Kirchhoffs law it is known that the emissivity is equal to the absorption and for a diffuse surface, the reflectivity is independent of outgoing and incoming directions. For this model any absorption, emission and scattering is ignored (hence the name of the model) only surface-to-surface radiation is considered.

The heat transfer is calculated according to the view factors. These are calculated automatically and accounts for the surfaces size, separation distance and orientation. The basis of the view factors can either be face-to-face or cluster-to-cluster. The cluster-to-cluster basis gathers surfaces into clusters and calculates a common view factor for each cluster. This option is suitable for complex geometry with a high number of surfaces. Since the model only has six surfaces it is chosen to use the face-to-face basis. This relates to the boundary conditions chosen for each wall, where only the two main walls were selected to participate in the view factor calculation, namely the heated wall and the glass. In this setting the number of faces per surface cluster was set to one, as each wall is considered as one surface.
There are two methods for calculating the view factors: Ray tracing and Hemicube. The Hemicube is more accurate than the Ray tracing method since it divides the surfaces into subsurfaces, calculate a view factor for each subsurface and sums them for the whole surface. The Hemicube

is recommended for large complex geometries, and since the model is simple it is chosen to use the ray tracing method and considered sufficient.

The reflected energy flux of a surface depends on the incident energy flux of its surrounding surfaces and it can be expressed as the energy flux from all the other surfaces. The reflected energy of a surface k is given by the Equation B.6, [Jiru, Teshome Edae and Tao, Yong-X and Haghighat, Fariborz, 2011].

$$q_{out,k} = E_k + \rho_k q_{in,k} \tag{B.6}$$

The amount of the incident energy from a surface j onto the surface k, is given by the view factor F_{jk}. In other words, the view factor can be expressed as the fraction of energy emitted by surface i directly on a surface k. For N surfaces, the incident energy flux is given by equation B.7

$$q_{in,k} = \sum_{j=1}^{N} F_{kj} q_{out,j} \tag{B.7}$$

Therefore, the radiosity of a surface k can be expressed by equation B.8.

$$q_{out,k} = E_k + \sum_{j=1}^{N} F_{kj} q_{out,j} \tag{B.8}$$

B.8 Boundary Conditions

- Inlet

The air inlet was set to be a velocity inlet since the velocity is known in advance. The velocity and the air temperature were set according to the measured values during the experimental study. As for the turbulent quantities of k (kinetic energy) and ϵ (dissipation rate) of the inlet, they are derived from empirical correlations among the turbulent intensity I, the length scale l and the inlet velocity u as they are presented in the equations B.9, and B.10.
The turbulence length scale was set to depend on the hydraulic diameter D_h (which was calculated to be 0.1337 m for a rectangular inlet) and the turbulence intensity was taken as the default value of the Ansys Fluent software equal to 5%.

$$k = \frac{3}{2}(u \cdot I)^2 \quad \text{with} \quad I = 0.16(Re)^{-1/8} \tag{B.9}$$

$$\epsilon = {C_\mu}^{3/4} \frac{k^{3/2}}{l} \quad \text{with} \quad l = 0.07 D_h \tag{B.10}$$

- Outlet

The outlet was modelled as a pressure outlet with the same turbulent quantities values as the inlet, taking into consideration the uncertainty if the flow is fully developed or not. Another benefit was that by using pressure outlet, its pressure is extrapolated from the interior. The back flow was not calculated during the experiments, so it was set to be normal to boundary, as an option for back flow direction specification method. Its temperature was set from the average temperature for each case of the experiments.

- Walls

The walls were taken as adiabatic walls without heat fluxes and no-slip shear conditions. This indicates that the air sticks to the walls and the velocity will be zero at the boundary walls. All the momentum would be lost when the fluid molecules hit the wall. Concerning the heaters, which were used to create a temperature distribution, they were set as having no-slip shear conditions and having a temperature range as they had during the measurements.

- Radiation

Regarding the boundary conditions for the radiation, only the surfaces that were defined previously to section B.7 on page 47 were used.

B.9 Discretization Scheme

The SIMPLE algorithm was used to couple the pressure and the momentum equations. The simulations used the second order upwind discretization scheme for all the convection and the viscous terms of the governing equation and the pressure. In order for the solution to be considered converged, the sum of the absolute normalised residuals for all of the cells in the domain was set to be less than 10^{-6} for the energy and 10^{-3} for all the other variables.

APPENDIX

C Electronic Appendix

This Appendix for this chapter is in a CD, which is attach and in this thesis.